Met Office

A Simple Prognostic based Convective Entrainment Rate for the Unified Model: Description and Tests

Forecasting Research Technical Report No: 617

May 2017

M. R. Willett and M. A. Whitall

Abstract

Many models struggle to capture aspects of tropical variability that are very directly related to the parameterisation of convection, such as the diurnal cycle and the intensity of precipitation. The entrainment rate used in a convective parameterisation is an extremely important factor in determining the model's mean climate, its variability and its predictive skill. However, the limitation of using a single entrainment rate results in a compromise between the different performance measures. We present a simple modification that allows the deep convective entrainment rate to vary over a realistic range of values by linking it to the amount of convective activity within the last several hours, as measured by a 3-dimensional prognostic based on surface convective precipitation. The underlying premise of the modification is that locations that have experienced high levels of recent convective activity will be populated with relatively large convective clouds that have low entrainment rates: conversely, locations that have experienced low levels of recent activity will be populated with relatively small convective clouds (if any) that will have high entrainment rates. We will show that this simple change, or using an increased but constant entrainment rate, are both able to deliver significant improvements to the representation of convection and tropical variability in both climate and NWP configurations of the Met Office Global Atmosphere model. However, whereas simply increasing the entrainment rate degrades the mean climate and forecast skill in the tropics, the additional degree of freedom introduced by the prognostic based variable entrainment rate does not significantly degrade the mean climate and forecast skill.

1 Introduction

Atmospheric moist convection cannot be fully resolved at horizontal, vertical and time resolutions used by current global models. It is therefore currently necessary (and will continue to be necessary for some time) to parameterise convection at global model resolutions. However, models that include parameterised convection always struggle to capture all the modes of tropical variability whilst maintaining an acceptable mean climate and acceptable levels of NWP performance. In particular the main issues often attributed to the representation of convection in the global model are:

- The diurnal cycle over tropical land is poorly represented with, in a time mean sense, convection starting and peaking too early in the day, and with the amplitude of the cycle being too large.
- The instantaneous spatial structure of tropical precipitation looks unrealistic: peak precipitation rates are too low and the precipitation is too spatially diffuse when compared with observations.
- The deepest convection is not deep enough yet there is a lack of mid-top convection.
- NWP forecasts at even very short forecast lead-times show limited skill in the forecasting of convection.

© Crown Copyright 2017

- The MJO is often too weak in medium- and long-range forecasts and climate simulations.
- There are large and systematic regional and seasonal biases in tropical rainfall in climate simulations, e.g. there is too little precipitation over India during summer.

Problems such as the diurnal cycle, instantaneous structure and depth of convection are clearly related to the parameterisation. However, it is worth stressing that features such as the south Asian monsoon and the MJO occur on temporal and spatial scales that are far removed from those at which convection is parameterised; it is therefore far from clear whether or not their poor representation is *solely* caused by the limitations in the representation of convection.

It could be argued that a potential source of these errors is that the convection scheme is too tightly coupled to the surface fluxes and CAPE (which is itself tightly controlled by the near surface properties), and too weakly coupled to large-scale dynamics and the free tropospheric humidity (which is itself coupled to the large-scale dynamics). This hypothesis is supported by Klingaman and Woolnough (2014) and Bush *et al.* (2015), who show that some modes of tropical variability may be improved by increasing the entrainment rate. Indeed, the 25% entrainment rate increase at GA6 (Walters *et al.* (2016)) was primarily motivated by this work. However, the use of a *single* entrainment rate results in a compromise between improving the variability and degrading the mean climate and NWP performance. Furthermore, studies of the diurnal cycle using models with cloud resolving resolutions (e.g. Stirling and Stratton (2011) and Del Genio and Jingbo (2009)) show that entrainment rates decrease during the day as convection deepens. It therefore seems likely that an additional degree of freedom in the entrainment rate is required in order to improve the variability in general, and the diurnal cycle in particular, without degrading the mean state.

The real atmosphere holds information about the state of convection (e.g. the number and size of convective clouds, distributions of temperature, humidity, momentum etc) on scales that are unresolved by the model. The unresolved state of the real atmosphere evolves according to the same physical laws as the resolved state and hence the unresolved state at a certain time will be strongly dependent on its state a short time earlier. Even the most cursory examination of a sequence of radar or satellite images will reveal that in the real atmosphere convection is autocorrelated for short time lags. The convection scheme, however, operates solely on the current *resolved* state of the atmosphere: it has no knowledge of the unresolved state and hence it has little ”memory” of recent convective activity other than that imparted onto the resolved scale. This is clearly a missing process within the current convection scheme. The potential importance of including some form of memory within the convection scheme is hinted at by Davies *et al.* (2009). They demonstrated that even in their very simple model of convection the timescale of convective ”memory” can have a very significant affect on the behaviour of the system (nb having no memory is equivalent to having memory but with a very short timescale). Convective ”memory” could be added to the model by the addition of one or more new prognostic variables that carry information about recent convective activity.

© Crown Copyright 2017

A number of enhancements to convective mass flux parameterisations have been suggested recently, aiming to address some of problems discussed above, and in particular to improve the diurnal cycle of convection over land. Kain (2004) link the cloud radius to the time-meaned large-scale vertical ascent such that greater vertical ascent results in a larger radius and hence smaller entrainment rates. Hohenegger and Bretherton (2011) link the entrainment rate to the precipitation at convective cloud base such that higher precipitation rates result in lower entrainment rates. The change resulted in an improved diurnal cycle of convection. Although they state that they do not add an additional prognostic, they use the precipitation rate meaned over the last hour which is in essence a new prognostic in all but name. They also used the (time-meaned) precipitation rate to control the cloud base mass flux and thermodynamic properties at cloud base, but noted that changing the entrainment has the largest impact. Mapes and Neale (2011) adds a new advected, unitless prognostic, org, that has the evaporation of precipitation as its source and decays over a three hour timescale. The prognostic, org, then controls the parcel ascent such that larger values reduce the entrainment rate and increase the cloud base mass flux. Their approach is similar to the "first and heuristic step" proposed by Piriou *et al.* (2007), linking the entrainment rate to a precipitation-evaporation-forced prognostic field. Motivated by a lack of sensitivity to environmental moisture and an excessive coupling between convection and large-scale dynamics in the IFS, Bechtold *et al.* (2008) replaced an entrainment rate that depended on large-scale moisture convergence with a rate that is dependent on the relative humidity such that higher humidities generate lower entrainment rates. All these changes reduce the entrainment rate in regions where deep convection would be expected (strong vertical ascent or high relative humidity) or more directly where convection has recently been active (time-mean precipitation or evaporation).

Based on CRM studies in Stirling and Stratton (2011), Stratton and Stirling (2011) suggested a different approach whereby the entrainment rate for deep convection is set to be inversely dependent on the boundary layer depth. They demonstrated that the diurnal cycle of convection over land was improved because the entrainment rate was increased during the development phase and reduced as deeper convection developed. The key result from the various studies cited above, that the diurnal cycle can be improved by replacing a fixed entrainment with a variable entrainment rate that responds to the state of the atmosphere, provides motivation for introducing an additional degree of freedom to the entrainment rate. The method used by Stratton and Stirling (2011), however, had the disadvantage of needing a land-sea split within the convection scheme to avoid shallow oceanic boundary layers constantly diagnosing high entrainment rates. Furthermore, it was not possible to implement in a GA configuration because it was susceptible to grid point storms over tropical rainforests that can have boundary layer depths similar to those over the ocean.

Finally, rather than altering the entrainment rate, Bechtold *et al.* (2014) were able to improve the diurnal cycle of convection over land by modifying the standard CAPE closure to take account of boundary layer forcing. Although such an approach could beneficially delay the timing of the peak rainfall, it is difficult to see how altering the closure could on its own prevent convection from

© Crown Copyright 2017

deepening too quickly.

Section 2 describes a new prognostic based entrainment rate that adds an additional degree of freedom to the entrainment rate via the use of convective memory. Like Hohenegger and Bretherton (2011), we take a simple approach in which the deep convective entrainment rate is varied as a function of the recent convective precipitation rate. The configuration that includes this will be referred to as ProgEnt. Section 3 describes the performance of this change relative to a GA7 control and also relative to a high entrainment configuration. Several areas where there is scope to improve the performance are identified and options within the convection scheme to address these are briefly discussed in Section 4. Section 5 provides a summary and conclusions, and briefly discusses future work.

2 Description of the Prognostic Based Entrainment Rate

2.1 New Convective Prognostic

There are clearly many ways in which we can introduce memory into the convection scheme. We choose here to define a new 3-dimensional model prognostic, $\bar{P}$, that is a measure of recent convective activity:

$$\frac{D\bar{P}\left(z\right)}{Dt} = \frac{\tilde{p}_{surf}^{cnv} - \bar{P}\left(z\right)}{\tau} \tag{1}$$

where $\tilde{p}_{surf}^{cnv}$ is a 3-dimension expansion of the instantaneous 2-dimensional surface convective precipitation rate and is defined as:

$$\tilde{p}_{surf}^{cnv} = C\left(z\right) \max\left[p_{min}, p_{surf}^{cnv}\right], \tag{2}$$

where the 3-dimensional function, $C\left(z\right)$, is set to 1 if convection is active at a given level and 0 if it is not (here, convection is defined as being “active” on any level where the convective temperature tendency, including the contribution from downdrafts / evaporation of precipitation, is non-zero). Non-precipitating convection contributes to $\bar{P}$ via a small nominal precipitation rate, p_{min}, which is set to $10^{-5}\,\mathrm{kgm^{-2}s^{-1}}$. $\bar{P}$ is fully advected with the large-scale flow and hence it is very directly coupled to the dynamics (possible implications are discussed in more detail later). This is possible because we have defined a 3-dimensional quantity. This approach is preferable to using a 2-dimensional field because it avoids the additional complexity and approximation involved in defining a steering level for the prognostic. τ, the e-folding time, is set to $3\,\mathrm{hours}$ (equivalent to a half life of about $2\,\mathrm{hours}$) in the results shown. It defines what we mean by ”recent” and it is the timescale on which the convective system is expected to have ”memory” which is not captured within the

© Crown Copyright 2017

large-scale fields. The choice of this timescale (and its implications) is discussed later.

2.2 Relating the Prognostic and Entrainment Rate

In reality populations of convective clouds develop and grow over a finite timescale of typically several hours. Regions with little recent convective activity would, if any convection were present, be expected to be populated with relatively small convective clouds that would be subject to relatively high dilution by entrainment. Regions with high-levels of recent convective activity would be expected to be populated with relatively large convective clouds that would be subject to relatively low dilution by entrainment.

However, with the UM's present deep convection scheme (e.g. the GA7 configuration), fully developed deep convective clouds can appear instantaneously (within a timestep) without the need to develop and grow. Part of the reason for this behaviour is that once deep convection is diagnosed, it is given an entrainment rate that is appropriate for fully developed deep convection. There is currently no mechanism for using high or intermediate entrainment rates.

However, the introduction of a convective prognostic, $\bar{P}$ which provides a fully advected 3-dimensional measure of recent convective activity, provides a mechanism to control the entrainment rate in a physically sensible manner. The prognostic is related to the entrainment rate such that locations that have had relatively little recent convective activity have higher entrainment rates, and locations that have had high levels of recent convective activity have lower entrainment rates. This is done by scaling the standard entrainment rate by the following factor:

$$F\left(z\right) = C_{grad} \log_{10}\left(\bar{P}\left(z\right) \frac{q_s^{ref}}{q_s^{LCL}}\right) + C_{int}, \tag{3}$$

where C_{grad} is a *negative* constant that determines how strongly the entrainment is related to the prognostic and C_{int} is an intercept. In the configuration presented here $C_{grad} = -1.1$, $C_{int} = -2.9$ and the scaling factor F is limited to the range 0.5 to 2.5. q_s^{LCL} is the specific humidity of the near-surface mixed-layer (this corresponds to the specific humidity of an undilute parcel-ascent at the Lifting Condensation Level, calculated in the convective diagnosis), and the reference value for normalisation is $q_s^{ref} = 20.0\,\mathrm{gkg}^{-1}$. The dependence on q_s^{LCL} accounts for the fact that temperature exhibits a strong control on precipitation rates; without this dependence equation (3) would always diagnose very high entrainment rates in mid-latitude conditions. Note that the scaling has a logarithmic dependence on $\bar{P}$; this reflects the fact that precipitation rates can vary over several orders of magnitude, but it is required that the scaling should only vary by a factor of ~ 5. The values of C_{grad}, C_{int} used in (3) were arrived at by using estimates of the range of tropical precipitation rates (from 3-hourly TRMM and model data) and associated entrainment rates (the lower limit being approximately half the current value used in deep convection and the upper limit being similar to values used by the shallow convection scheme). Values of F for a range of values of $\bar{P}$ and q_s^{LCL}

© Crown Copyright 2017

are shown in Table 1. It should be noted that the precipitation rates used here represent averages over the timescale $\tau = 3$ hours, and over a global model grid-box $\Delta x \sim$ 10–100km and hence they are considerably smaller than the expected instantaneous local precipitation rates occuring within convective cells.

$\bar{P}$			F	
$\mathrm{kgm^{-2}s^{-1}}$	$\mathrm{mmhour^{-1}}$	$\mathrm{mmday^{-1}}$	$5\,\mathrm{gkg^{-1}}$	$20\,\mathrm{gkg^{-1}}$
10^{-6}	0.0036	0.09	2.5 (3.0)	2.5 (3.7)
10^{-5}	0.036	0.86	1.9	2.5 (2.6)
10^{-4}	0.36	8.64	0.8	1.5
10^{-3}	3.6	86.40	0.5 (-0.3)	0.5 (0.4)

Table 1: Table of entrainment rate scaling F as function of $\bar{P}$ and saturated humidity values at the LCL of $5\,\mathrm{gkg^{-1}}$ and $20\,\mathrm{gkg^{-1}}$ at the LCL. The values in brackets indicate the value of F before the minimum and maximum limits have been applied.

The factor, F, is used to scale the standard deep convection entrainment rate profile, i.e.:

$$\epsilon\left(z\right) = F\left(z\right) f_{dp} 4.5 g \frac{\rho\left(z\right) p\left(z\right)}{P_0^2} \tag{4}$$

where p is pressure, p_0 is the pressure at the surface and ρ is density. The profile is identical to that originally used in Gregory and Rowntree (1990) apart from the additional tuning parameter f_{dp} that is set to 1.13 in GA7 but to 1.0 in ProgEnt because the prognostic based scaling factor F makes it redundant. Note that in the convection scheme, the fractional entrainment rate ϵ is computed in pressure vertical coordinates (units Pa^{-1}); the factor $g\rho$ has been added in eq (4) to convert the units to m^{-1}. The entrainment rate profile of GA7 and the minimum and maximum entrainment rates of ProgEnt (using (4) and assuming a fixed lapse rate) are shown in Figure 1 (also shown are the HiEnt and LoEnt profile that are defined later). The range of entrainment rates available in ProgEnt is consistent with those derived in high resolution simulations especially at low-levels. For example, at $850\,\mathrm{hPa}$ / $\sim 1.5\,\mathrm{km}$ ProgEnt has a range of 0.2 to $1.0\,\mathrm{km^{-1}}$ which compares well with values of 0.3 to $1.3\,\mathrm{km^{-1}}$ shown in Stirling and Stratton (2011)[1] and 0.2 to $0.7\,\mathrm{km^{-1}}$ shown in de Rooy *et al.* (2013)[2]. The decline of entrainment rate with height usually seen in cloud resolving model estimates is built into both GA7 and ProgEnt via the pressure dependence. It is worth noting that the scaling factor, $F\left(z\right)$, can vary with height and hence the entrainment rate for any particular ascent is only bounded by the minimum and maximum values.

2.3 Discussion

It can be seen in eq (1) that the convective prognostic, $\bar{P}$ is, apart from an additional height dependence, essentially a time-smoothed convective precipitation rate. Examples of the 3-hour mean

[1] Taken from their figure 7a
[2] Taken from their figure 8c

© Crown Copyright 2017

convective precipitation rate and $\bar{P}$ at a range of levels are shown in Figures 2 and 3 - the similarity at low levels is readily apparent. At higher levels $\bar{P}$ captures regions of the deepest convection. The very direct link to convective precipitation confers some notable benefits. We know the climatology and the typical range of values that $\bar{P}$ will take. $\bar{P}$ is also well constrained by the global water and energy budgets and is not susceptible to long terms drift (unless of course there is drift in convective precipitation). Comparison of the $\bar{P}$ fields from N96, N320 and N768 case study runs suggests that the range and distribution of $\bar{P}$ is not very sensisitive to horizontal resolution[3] and hence the same configuration of ProgEnt may be used over a wide range of horizontal resolutions.

Eq (1) describes how $\bar{P}$ evolves over time. To get an expression for how the entrainment rate scaling, $F(z)$, evolves we rearrange (1) to give:

$$\frac{D \ln \bar{P}(z)}{Dt} = \frac{1}{\tau}\left(\frac{\tilde{p}_{surf}^{cnv}}{\bar{P}(z)} - 1\right), \tag{5}$$

and rearrange (3) to give:

$$\ln \bar{P}(z) = \frac{\ln(10)}{C_{grad}}\left(F(z) - C_{int}\right) - \ln \frac{q_s^{ref}}{q_s^{LCL}} \tag{6}$$

Substituting (5) into (6) gives the following expression for the evolution of $F(z)$:

$$\begin{aligned} \frac{DF(z)}{Dt} &= \frac{C_{grad}}{\tau \ln(10)}\left[\frac{\tilde{p}_{surf}^{cnv}}{\bar{P}(z)} - 1 + \tau \frac{D}{Dt}\left(\ln \frac{q_s^{ref}}{q_s^{LCL}}\right)\right] \\ &= \frac{C_{grad}}{\tau \ln(10)}\left[\tilde{p}_{surf}^{cnv}\frac{q_s^{LCL}}{q_s^{ref}} \exp\left(-\frac{\ln(10)}{C_{grad}}\left(F(z) - C_{int}\right)\right) - 1 + \tau \frac{D}{Dt}\left(\ln \frac{q_s^{ref}}{q_s^{LCL}}\right)\right] \end{aligned} \tag{7}$$

In the absence of precipitation $\bar{P}$ will decay exponentially over time with an e-folding time τ, i.e. $\bar{P}(t) = \bar{P}(0)\exp(-\frac{t}{\tau})$. The scaling applied to the entrainment rate, F, is a logarithmic function of $\bar{P}$ and therefore in the absence of precipitation and assuming that there is no change in q_s^{LCL} it will increase *linearly* with time, i.e. $F(t) = F(0) - \frac{C_{grad}t}{\tau \ln(10)}$ until it reaches it maximum value (note that C_{grad} is negative and hence the multiplier of t is actually positive). Over the timescale τ, F will increase by $\frac{C_{grad}}{\ln(10)} \approx 0.5$.

In the prognostic equation (1) τ is a characteristic physical timescale that defines what is meant by "recent" in our measure of recent convective activity, $\bar{P}$. It defines the timescale on which the convective system is expected to have "memory", but what this physically means and what value it should have depends on how it is used. The prognostic, $\bar{P}$, is used to control the entrainment rate and the entrainment rate is expected to be inversely proportional to cloud radius (e.g. Simpson and Wiggert (1965)). Therefore, although it is based on surface precipitation rate, we are using $\bar{P}$

[3]There probably should be more sensitivity then there actually is as finer scales are resolved. Lack of such sensitivity possibly suggests that the model is unable create and persist convective systems at fine scales.

© Crown Copyright 2017

in combination with q_s^{LCL} in (3) as a proxy for cloud size. The decay timescale, τ, should therefore be related in some sense to convective cloud lifetime. Individual convective cloud lifetimes are quite short, $\sim 1000\,\mathrm{s}$, but this may extended to $\sim 1\,\mathrm{hour}$ in more organised situations (Wilson *et al.* (1998)). Mesoscale convective systems can persist for timescales of several hours or even more than a day (e.g. Houze Jr (2004) and Machado *et al.* (1998)) (or several days if we also consider tropical cyclones). But these longer time-scales arise because of the feedback between convection, which needs to be parameterised by the model, and the large-scale flow, which is resolved. These timescales put loose, and hence not very useful, bounds on the value that τ should take.

However, what we really require is not a timescale of an individual cloud or an MCS, but something that is harder to measure - a timescale for the mean cloud size within an ensemble of convective clouds including unresolved or unrepresented processes that directly or indirectly affect convective cloud size, but excluding resolved processes that affect convective cloud size. Unresolved processes that will affect cloud size would include the generation of downdraughts and cold pools; these processes are very directly related to precipitation and hence supports the use of precipitation as the source for $\bar{P}$. τ much more naturally represents a decay timescale than a growth timescale, but to put some context on its value, observations of transitions between between congestus and deep convection were shown by Hohenegger and Stevens (2012) to typically occur on timescales of $2\,\mathrm{hours}$ over land and $4\,\mathrm{hours}$ over the oceans in the tropics. Perhaps the most useful estimate for what value τ should take comes from Davies *et al.* (2013). They analysed the effects of forcing a CRM on a range of timescales and found that convective memory (behaviours which are independent of the domain-mean profiles and forcings) is important on forcing timescales of $3-12\,\mathrm{hours}$. From a practical point of view we require that $\bar{P}$ can capture the diurnal cycle and then clearly $\tau \ll 24\,\mathrm{hours}$, and furthermore from a numerical perspective we require that $\bar{P}$ is insensitive to timestep level noise in convective precipitation and hence $\tau \gg \Delta t$ where Δt is the model timestep. Given the limited evidence, our practical constraints and the results of some sensitivity tests, a value of $\tau = 3\,\mathrm{hours}$ appears reasonable and is used for the results presented in this report. Such a value is consistent with other parameterisations that include an element of convective memory, e.g. Mapes and Neale (2011) use a damping timescale of $3\,\mathrm{hours}$ for their org parameter and Hohenegger and Bretherton (2011) use $1\,\mathrm{hour}$ mean precipitation to calculate entrainment.

Should we expect the time-mean precipitation from a plume model to be dependent on the entrainment rate as described in (3)? We test this by applying a simple entraining plume model to idealised but realistic atmospheric profiles and varying the entrainment profile. The idealised temperature profiles were set to follow a moist adiabat from the surface up to a defined tropopause but then adjusted to give a prescribed amount of CAPE. The relative humidity was set to a fixed value of $90\,\%$ and hydrostatic balance was imposed. The plume was set to be saturated at the surface with a buoyancy of $0.2\,\mathrm{K}$ and allowed to ascend until its buoyancy became negative. The microphysics for the plume was taken from the UM's convection scheme and CAPE closures with a range of fixed timescales were applied. The variation of the plume-model's precipitation rate as a

© Crown Copyright 2017

function of the prescribed entrainment rate is shown in figure 4 for idealised tropical and mid-latitude cases and in both cases they can exhibit a similar log-linear relationship as in (3). The precipitation rate from the simple model will be dependent on the CAPE and relative humidity (of which (3) obviously has no knowledge) so in general we would not expect an exact match with the precipitation rate in (3). Furthermore (3) is designed to operate on a time-mean precipitation rate whereas the simple plume model predicts an instantaneous rate from a prescribed environment profile. The simple model also does not include processes such as subcloud evaporation and downdraughts. Notwithstanding this, the functional form of the empirical relationship between entrainment and time-mean precipitation rate in (3) is consistent with the relationship seen in a simple entraining plume model with a CAPE closure. This result supports the assertion, which is implicitly made in this scheme, that the (time-mean) precipitation rate is a function of the entrainment rate and hence that it is reasonable to invert that relationship and use the (time-mean) precipitation to estimate the entrainment rate.

It is obvious from (1) and (3) that if $\tilde{p}^{cnv}_{surf}$ is greater [less] than $\bar{P}$ then the entrainment rate will reduce [increase] and the inferred cloud size will increase [decrease]. Furthermore, if $\tilde{p}^{cnv}_{surf} = \bar{P}$ then the entrainment rate will be in a steady state; this steady state will exist if the following condition holds:

$$F = C_{grad} \log_{10} \left(\tilde{p}^{cnv}_{surf}\left(F\right) \frac{q^{ref}_s}{q^{LCL}_s} \right) + C_{int}$$

Therefore, the relationship between the $\bar{P}$ and the entrainment rate scaling, F, in (3) does not in anyway impose a relationship between the precipitation and entrainment in the parameterisation, but rather it characterises an equilibrium state for the entrainment rate (and hence inferred cloud size). It should be noted that in the control the entrainment rate is fixed in time and hence is always in a steady state.

It is desirable to advect $\bar{P}$ with the large-scale flow because the resolved and unresolved properties of a parcel of air, which in combination will describe convective activity within the parcel, would also be advected by the large-scale flow. Many forecasting applications make use of this fact by assuming that features such as thunderstorms are horizontally advected by a steering level wind (e.g. Met Office (1996)). Advection obviously allows $\bar{P}$ to be non-zero at locations that have not experienced recent convection because non-zero values can be advected in from elsewhere: ProgEnt does not force convection to operate at such locations but rather it "encourages" convection to develop via a reduced entrainment rate. The vertical advection of $\bar{P}$ will in theory act to encourage convection where there is large-scale vertical ascent and discourage convection where there is descent. This behaviour is desirable but idealised tests suggest that it is very small compared to the large effect that the advection of temperature and humidity has upon the development of convection.

ProgEnt has some similarities to the scheme described in Mapes and Neale (2011) but there

© Crown Copyright 2017

are some important differences. They use the *evaporation* of precipitation, rather than convective precipitation, as the source for their unitless org prognostic. Some benefits of using precipitation were noted earlier. A potential problem with using evaporation is that the amount of parameterised evaporation in the model is not well constrained with observations. A particular problem in the MetUM is that the evaporation of convective precipitation has a strong dependence on a diagnostic convective cloud area which is a very uncertain quantity. Their dependence of entrainment rate on their org prognostic differs in the detail but is in the same sense, i.e. greater organisation/increased activity leads to decreased entrainment rates. Another notable difference is that we include a dependence on q_s^{LCL} in (3) which allows the entrainment scaling to function, i.e. to give a broad pdf of entrainment rates, over a broad range of temperatures. Some of the other differences, such as a fully advected $\bar{P}$ in ProgEnt and advecting org using a steering level in Mapes and Neale (2011), are likely to be of secondary importance.

3 Performance of ProgEnt

The assessment of ProgEnt has been split into three parts. Firstly the behaviour of convection in ProgEnt will be assessed and contrasted to GA7 using detailed diagnostics from an NWP case study, SCM simulations of TOGA-COARE and a 20-year AMIP simulation. For the AMIP tests the analysis will concentrate on the four different tropical regions defined in table 2. The second and third parts look at the mean climate in the AMIP test and performance in 24 NWP case studies respectively using more standard methods.

Name	W	E	S	N
West Africa	-10	10	5	15
Central Africa	15	25	-10	10
Maritime Continent	100	120	-5	5
Warm Pool	120	160	0	10

Table 2: Definition of tropical regions used in figures 7, 8, 25, 21

In order to determine whether the benefits of ProgEnt arise from having an extra degree of freedom in the entrainment rate, or simply by having an increased mean entrainment rate, an additional configuration, HiEnt, has also been tested. HiEnt is identical to the GA7 control except that its entrainment rate has been increased by 55% ($f_{dp} = 1.75$ compared to 1.13 in GA7). This value was chosen because, as will be shown, it gives a similar diurnal cycle improvement to ProgEnt. In the SCM tests, a low entrainment configuration, LoEnt, has also been run where the entrainment rate has been reduced by 33% ($f_{dp} = 0.75$).

© Crown Copyright 2017

3.1 Convection Assessment

3.1.1 Entrainment Rates and Depth of Convection

Figure 5 shows histograms of entrainment rates at $250\,\mathrm{hPa}$, $500\,\mathrm{hPa}$, and $850\,\mathrm{hPa}$ from SCM simulations of TOGA-COARE. GA7, HiEnt and LoEnt each have only a single entrainment rate for deep convection at any given pressure level. In contrast, ProgEnt produces a broad spectrum of entrainment rates, with the highest entrainment rates exceeding those of HiEnt, whilst its lowest entrainment rates are lower than LoEnt. There is a factor of almost 5 between its lowest and highest values, which demonstrates that the allowed range of entrainment rates in ProgEnt is almost fully explored in this one case. Unsurprisingly, the values of entrainment rate are consistent with those in figure 1. At all levels there is a peak in the PDF for ProgEnt that is very close to the single peak in GA7. Time-height profiles of entrainment rate for the four SCM simulations are shown in figure 6. In GA7, HiEnt and LoEnt the deep convection scheme's entrainment rates are clearly fixed functions of height irrespective of the depth of convection (in LoEnt shallow convection, which uses relatively high entrainment rates, is occasionally diagnosed). In ProgEnt the entrainment rate at any given level varies with time. When convection is relatively shallow (implying shallow or congestus type convection) the entrainment rates are relatively high and when convection is deeper then entrainment rates are relatively low. Noting that we would expect cloud size to scale inversely with entrainment rate, this behaviour seems not just reasonable but desirable. Furthermore, when convection becomes shallower or deeper the entrainment rates tend to smoothly increase or decrease (notwithstanding the convective intermittency which is a feature common to all configurations).

The increased range of entrainment rates used by ProgEnt leads to an increased spread in the termination levels for deep convection. This can be seen not only in the SCM simulations (not shown) but also in the full model simulations; e.g. figure 7 shows profiles of the frequency of termination for deep convection from the 20-year AMIP simulation using GA7, ProgEnt and HiEnt for four different tropical regions. In GA7 the majority of deep convection events terminate in the upper troposphere with a relatively small number terminating in the mid- or lower-troposphere. This suggests that GA7 rarely generates congestus like convection and almost never generates shallow like convection, which is consistent with it using a fixed low entrainment rate that is most appropriate for deep convection. The representation of congestus was noted as a weakness of GCMs including the MetUM in Willett *et al.* (2008). HiEnt has peaks in termination frequency at $\sim 2.5\,\mathrm{km}$, $5-6\,\mathrm{km}$ and in the upper troposphere at $\sim 12\,\mathrm{km}$, which may be interpretated as shallow, congestus and deep convection respectively. The depth of deep convection in HiEnt, however, is typically $\sim 2\,\mathrm{km}$ less deep than in GA7. The additional degree of freedom in the entrainment rate results in ProgEnt being able to create shallow and congestus convection in a similar manner to HiEnt (i.e. peaks in termination at $\sim 2.5\,\mathrm{km}$, $5-6\,\mathrm{km}$) but still being able to generate deep convection that is as deep or deeper than that in GA7. The ability of ProgEnt (and HiEnt) to generate shallow and congestus convection via the deep convection scheme is desirable as it will aid the representation

© Crown Copyright 2017

of transistions from shallow to deep convection (this may be especially important over tropical land where the shallow convection scheme itself is very rarely diagnosed[4]). The differences among the simulations in terms of mean convective mass flux are much more subtle (Figure 8), but compared to GA7, ProgEnt's deep mass flux profile reduces more rapidly with height at levels where it has a higher termination frequency.

Mid-level convection contributes a large proportion of the mass flux over tropical land (since deep convection makes up about only half of the total and shallow convection will only operate at lower levels and is very infrequently diagnosed over land). This is especially true at above $14\,\mathrm{km}$ where the mass flux is coming almost exclusively from mid-level convection. As we shall see, mid-level convection is the dominant type in the most dynamically active areas over tropical land. Note that mid-level convection is identical in GA7, ProgEnt and HiEnt.

3.1.2 Cloud

Figure 9 compares profiles of cloud frequency from the 20-year AMIP simulations generated using the CALIPSO simulator with CALIPSO observations. For the tropical regions shown here, all configurations have too little high level cloud (that is cloud higher than $7\,\mathrm{km}$) except for GA7 over the warm pool: it should be noted that averaged over the whole tropics there is actually very little bias in the *amount* of high level cloud in GA7 by this measure (not shown). In general the *amount* of high level cloud is reduced in both ProgEnt and HiEnt relative to GA7 (this can also be directly seen in the comparisons with ISCCP (not shown) and indirectly via the reduction in OLR in figure 29) possibly because a greater proportion of deep convective events are terminating at lower levels. The high level cloud in GA7 is typically too low in height with the peak being $\sim 1\,\mathrm{km}$ too low. Neither ProgEnt or HiEnt significantly shift the height of the peak cloud amount but the distribution about the peak does change. In HiEnt the distribution of cloud about the peak has shifted slightly downward which is consistent with it having fewer events reaching the highest levels. In ProgEnt the distribution of cloud about the peak has shifted upwards slightly which is consistent with it have more events reaching the highest levels. The upward shift in high cloud seen in ProgEnt is desirable and addresses a bias that experience suggests is difficult to address by other means. The changes in high level cloud are consistent with the changes in the cloud condensate increments seen in the case studies (e.g. figures 14 and 15), with ProgEnt detraining more condensate than GA7 above $15\,\mathrm{km}$ and HiEnt detraining less.

GA7 has too little mid-level cloud between $4\,\mathrm{km}$ and $7\,\mathrm{km}$ and despite both ProgEnt and HiEnt terminating significantly more events at these levels in the AMIP test there is no significant change in the cloud. The convective cloud condensate increments from the case studies show that ProgEnt is actually detraining less condensate than GA7 (and has a more negative water vapour increment) and HiEnt is detraining more at these levels (but this also has a more negative water vapour incre-

[4]The shallow scheme is primarily designed to operate within trade cumulus regimes where there is a clear low-level inversion. Low-level inversions would not usually be expected over tropical land and hence the diagnosis, which uses an undilute parcal ascent, rarely diagnoses shallow convection at such locations.

© Crown Copyright 2017

ment). However, in both cases the total increment to cloud condensate is essentially unchanged because other processes, predominantly the large-scale microphysics, cancel out the changes from convection.

GA7 also has a lack of cloud below $4\,\mathrm{km}$. Both ProgEnt and HiEnt have more events terminating at these levels and an associated increase in the amount of detrained condensate (figures 14 and 15) and an increase in cloud fraction increments (not shown), but there is surprisingly little change in the cloud frequency at these levels. This perhaps suggests that for liquid cloud at low and mid-levels, the large-scale microphysics is the dominant process controlling the amount of cloud.

3.1.3 Temperature Structure

Since ProgEnt (and HiEnt) has altered where convection terminates and the cloud structures, we may expect the temperature structure to change and this is indeed the case. In fact the main negative signal of ProgEnt in the AMIP test is a cooler lower tropical troposphere and a warmer upper tropical troposphere (figure 16). The NWP case studies develop a very similar change in the temperature structure (figure17), albeit smaller in magnitude, throughout the troposphere, and they may be used to understand these differences. In particular, it is instructive to examine how ProgEnt changes the temperature increments (figures 10 and 11) and the convective mass flux (figure18). The warming of the upper-levels is initially caused by an increase in convective heating, which is associated with an increase in mass flux, and by a reduction in long-wave cooling, which is consistent with the reduction in high cloud. As the forecast proceeds, the upper-levels become warmer, which increases the bulk stability of the troposphere and reduces the mass flux until it is similar to the control. It should be noted that even though the convective mass fluxes are very similar, the effects of the mass flux on the environment can differ because of the modified environmental temperature structure and different convective parcel properties[5]. The situation in the lower troposphere is more complex during the first day of the case studies with changes in the increments from convection, long-wave radiation and large-scale microphysics all contributing to a net cooling. At longer timescales the cooling relative to GA7 is dominated by increased long-wave cooling perhaps partly due to the reduced amount of high-level cloud.

The tropical tropopause warm bias at 100 hPa ($\sim 16.5\,\mathrm{km}$) is almost $1\,\mathrm{K}$ warmer in AMIP simulation of ProgEnt than in GA7. The timescale for this bias to develop is much longer than the 5-days used in the case studies but ProgEnt does warm slightly more quickly than GA7 at these levels. As it stands the increased warm bias at 100 hPa and the associated moistening of the stratosphere would be problematic from a tropical tropopause layer (TTL) and atmospheric chemistry point of view (e.g. Hardiman *et al.* (2015)).

It should be stressed that the tropical troposphere is essentially in convective-radiative equilib-

[5]The convective increment is $\rho\frac{\partial\phi^E}{\partial t} = M\left(\frac{\partial\phi^E}{\partial z} + \mu(\phi^P - \phi^E) + \delta(\phi^R - \phi^E)\right)$ where ρ is the air density, ϕ is a scalar, M is the mass flux, μ and δ are the mixing and forced detrainment rates, and the superscripts E, P and R indicate the properties of the environment, the convective parcel and the air undergoing forced detrainment respectively.

© Crown Copyright 2017

rium and hence the temperature structure is to a large degree controlled by the cloud. This perhaps explains how the temperature structure evolves in HiEnt. HiEnt produces less convective heating in the upper tropical troposphere than ProgEnt and on NWP timescales the temperature structure at these levels does not diverge far from GA7 and certainly less than differences between ProgEnt and GA7. However, in the AMIP tests HiEnt develops an upper level warm bias $\sim 1\,\mathrm{K}$ larger than that in ProgEnt. This is probably caused by HiEnt reducing the upper level cloud more than ProgEnt and the consequential change to the radiative heating (presumably by reduced LW cooling from cloud tops at upper levels) acts over much longer timescales than the convective heating. It is likely that the effect that convection has on the cloud through its increments to cloud condensate and fraction, and the response to these from other processes, is at least as important to the temperature structure at longer timescales (if not more so) as the convective increments to temperature (noting of course that not only are they interdependent within the convection scheme but also that they will feedback on one another).

3.1.4 Precipitation Intensity

Figures 19 and 20 compare the instantaneous[6] precipitation rates from TRMM 3B42, with a 36 hour forecast from an N320 case study from GA7, ProgEnt and HiEnt over the west Pacific, south-east Asia and Australia, and Africa and the Atlantic respectively. TRMM has convective systems that are coherent and show peak precipitation rates of 8 to 32 mmhr^{-1}, whereas the GA7 control has convection that is too weak with peak precipitation rates of typically 2 to 4 mmhr^{-1} and lacks coherent structure; this is entirely consistent with the assessment of the operational model in section 1. ProgEnt has more convective structure than the control, less light precipitation and more heavier precipitation, and hence it looks subjectively more similar to TRMM. HiEnt looks fairly similar to GA7 but it does generate higher peak precipitation rates than are seen in GA7. For a more objective analysis we follow Martin *et al.* (2017) in figure 21 and compare the precipitation rates from 4-months of AMIP simulations using GA7, ProgEnt and HiEnt, with GPCP for the four tropical regions. The results are consistent with the subjective analysis of the case study. GA7 produces precipitation rates that are systematically too low in all four regions. Again ProgEnt produces rates that are systematically higher and in general are in better agreement with the observations, although in the maritime continent and central Africa cases the rates are now slightly higher than those in GPCP. HiEnt also produces precipitation rates that are systematically higher than GA7 but in the case of the maritime continent and especially the warm pool the rates are significantly higher then those in GPCP.

[6]The TRMM 3B42 produces an estimate of precipitation rate every 3 hours but the rates should be interpreted as instantaneous (Huffman *et al.* (2007)). The precipitation rates from the case studies are formed in the same manner as for operational NWP, i.e. 1 hour mean rates for convective precipitation and truly instantaneous rates from large-scale precipitation.

© Crown Copyright 2017

3.1.5 Diurnal Cycle

In the NWP case study the spatial coverage of instantaneous light precipitation at around local noon over Africa in GA7, and perhaps to a lesser extent in HiEnt, is much larger than seen in TRMM (figure 20). This suggests that the main problem with the diurnal cycle of convection in GA7 is not that precipitation is peaking too early in the day in locations where convection should be active, but rather *precipitating* convection is developing at far too many locations. This is confirmed by comparing a 5-day Hovmuller plot of precipitation for an east-west section of Africa from the Atlantic coast to the Ethiopian highlands from the NWP case study from GA7 (Figure 23a) with that from TRMM (Figure 22). The precipitation in TRMM is dominated by westward moving mesoscale convective systems (MCSs) with very little evidence of a strong diurnal cycle. GA7 does produce a strong westward propagating MCS (and some spurious looking eastward moving systems[7]) - dynamically active areas are highlighted by the vertical velocity contours. Superimposed on top of the MCSs is a very strong diurnal cycle in precipitation across almost all of the domain, peaking at around local noon. Most of the precipitation associated with the westward propagating MCS actually comes from the mid-level convection scheme with some additional contribution from the large-scale precipitation (Figure 23). The spurious diurnal cycle in the precipitation, however, is generated by the deep convection scheme. The deep convective precipitation is only weakly modulated by the passage of the MCS if at all. Figure 23f shows the average depth of deep convection when present - again the depth of deep convection is only very weakly modulated by the passage of the MCS.

The Hovmuller plots for ProgEnt are shown in figure 24. ProgEnt generates the MCS in a similar manner to GA7 with again most of the precipitation coming from mid-level convection (which is unchanged between GA7 and ProgEnt). Within the dynamically active areas the amount of deep convective precipitation and the depth of deep convection is actually quite similar to that in GA7. In the less active areas deep convective precipitation is significantly reduced with respect to GA7. The net result is that the passage of the MCS modulates the deep convective precipitation much more strongly in ProgEnt than in GA7. Outside of the dynamically active areas there are actually more deep convective events with ProgEnt but they are significantly less deep than those with GA7 (compare figures 23f and 24f): furthermore, with ProgEnt deep convection tends to gradually deepen during the day, which seems realistic, whereas in GA7 the deep convective events start deep in the morning and stay deep until deep convection stops in the late afternoon.

Improvements in the diurnal cycle can also be seen in the climate simulations. Figure 25 shows the diurnal cycle of precipitation for the regions defined in table 2 for each season for TRMM, GA7, ProgEnt and HiEnt. Over tropical land GA7 clearly exhibits the errors in the diurnal cycle of convection typically seen in GCMs - a peak in precipitation that occurs too early in the day, too little overnight precipitation and an excessive peak-to-trough amplitude. Over west Africa, ProgEnt delays the peak in the diurnal cycle by between 3 and 6 hours which very significantly improves the agreement with TRMM: the precipitation is beneficially increased in the late-afternoon and early

[7] Similar features have been also been noted in the operation global model.

© Crown Copyright 2017

evening, but it is not always maintained into the early morning. A similar response is also seen in areas such as the southwest US and Mexico in JJA, and northern Australia in DJF. Over central Africa, there is little systematic delay in the peak, but the magnitude of the peak is reduced and the overnight precipitation is increased which both improve the agreement with TRMM. Similar behaviour is seen in other very moist regions such as the Amazon. The ability of ProgEnt to suppress convection, and in particular the depth of convection, through high entrainment rates may be limited in such regions because of very high background humidities - this hypothesis is supported by the lack of deep convection terminating at low levels ($< 3\,\mathrm{km}$) over central Africa (Figure 7). In both GA7 and ProgEnt there is a marked drop in the precipitation rate in the late afternoon before it recovers later in the evening - this is likely to be caused by an inconsistency between deep convection, which is active during the day, and mid-level convection, which is active at night.

Over tropical oceans, as exemplified here by the west Pacific warm pool, there is a diurnal cycle in convection that is driven in reality by the diurnal cycle in the SSTs, which is *not* represented in the models shown here, and by the diurnal cycle in the radiative heating/cooling of the atmosphere, which is represented in the models. Despite the lack of diurnal cycle in the SSTs, both GA7 and ProgEnt are able to capture the diurnal cycle over the west Pacific warm pool.

3.1.6 Madden-Julian Oscillation

Surprisingly, ProgEnt has little or no clear impact on the representation of the MJO. The strength of the MJO in terms of the OLR is slightly weakened but this is almost certainly because the reduction in high cloud results in less variance in OLR.

3.1.7 African Easterly Waves

As hinted at when comparing figures 23 and 24, in the AMIP simulations ProgEnt has beneficially more and systematically slightly stronger African Easterly waves than GA7 (Figure 26). This may be because the improved diurnal cycle is less disruptive to the waves or because ProgEnt provides stronger coupling between convection and dynamics. HiEnt (not shown) tends to lie between GA7 and ProgEnt for most of the AEW statistics.

3.2 Mean Climate

The climate performance of ProgEnt has been assessed using the standard 20 year AMIP test. In general, ProgEnt improves the annual mean precipitation over tropical oceans (figure 27). There are substantial reductions in the wet biases over the west Pacific, south Pacific convergence zone (SPCZ) and the Indian ocean. The magnitude of the wet-dry dipole in the tropical Atlantic is reduced. There is however, a detrimental increase in the strength of the ITCZ in the east Pacific. The changes over land are mostly relatively small but there is a reduction in the wet bias over the Andes and a

© Crown Copyright 2017

substantial reduction in the dry bias over the Maritime Continent land[8]. Overall ProgEnt reduces the global spatial RMSE of the annual mean precipitation and the RMSE of each individual season is also reduced (not shown). The tropical oceanic areas with reduced wet biases also tend to have beneficial increases in OLR (figure 29) and beneficial reductions in OSW (figure 28). There are increases in OLR over tropical land but the change in OSW over land is less consistent. The global mean OLR has increased by $0.8\,\mathrm{Wm}^{-2}$ and the OSW has reduced by a similar amount. Overall, as measured by the spatial RMSE, these changes are neutral or slightly beneficial.

In contrast to ProgEnt, HiEnt increases the wet biases over the West Pacific and SPCZ. The dry bias over the Maritime Continent is increased but there is actually little change relative to GA7 over Maritime Continent land. The improvements to the wet-dry dipole in the tropical Atlantic are quite similar to those in ProgEnt. Overall HiEnt increases the global mean spatial RMSE of the annual mean precipitation and the RMSE of each individual season. Whereas ProgEnt had a near neutral impact on the OLR and OSW, HiEnt significantly degrades them.

The impact of ProgEnt and HiEnt relative to GA7 for a wide range of metrics measuring mean climate is summarised in figure 30. With ProgEnt, the only metrics that are consistently degraded are the zonal-mean temperature ones; this is discussed in section 3.1.3 (in figure 30 ProgEnt also shows a degradation in zonal-mean zonal wind in DJF, but not in JJA, or in the meridional winds). As discussed above, the tropical oceanic precipitation is consistently improved. As measured by this range of metrics, ProgEnt has a near neutral impact on the mean climate (i.e. the "overall assessment" metric is very close to one). In contrast, HiEnt degrades the tropical oceanic precipitation, winds and zonal-mean streamfunction and overall degrades the mean climate.

3.3 NWP Performance

The NWP performance of ProgEnt has been assessed using the standard set of 24 N320 case studies. It is worth noting that the ProgEnt runs are slightly disadvantaged in case studies because the convective prognostic, $\bar{P}$, needs to spin up during the early part of the forecast.

Figure 31 shows the change in root mean square error (RMSE) of the NWP index parameters with respect to observations and analyses for ProgEnt relative to GA7. The large increase in the RMSE of 500 hPa geopotential heights falls off rapidly with forecast time; this is primarily caused by an increase in bias, which itself is caused by a cooler lower troposphere, rather than random error. The tropical winds are also degraded especially with respect to analyses. Despite the degradation at shorter forecast times, by T+120 the impact of ProgEnt is close to neutral. In contrast HiEnt clearly has a much larger detrimental affect on the forecast than ProgEnt (compare figures 31 and 32) with much larger errors appearing in the tropical winds (figures 33 and 34).

[8]The substantial increase in rainfall over the Maritime Continent land warrants further investigation to understand the mechanism for this change. It is likely that local effects (e.g. changes to the diurnal cycle or land-sea breezes) are contributing to the changes over the Maritime Continent land because similar increases in precipitation can also clearly be seen over Cuba, Hispaniola and Panama with ProgEnt at N216 (they are barely resolved at N96) despite the changes in large-scale circulation in this region being much smaller than for the Maritime Continent.

© Crown Copyright 2017

4 Scope for Improving the Performance of ProgEnt

As we have seen in section 3, ProgEnt increases the tropical temperature biases by cooling at mid-levels and warming at upper levels. The same changes in diabatic heating and cloud that are driving the changes in temperature structure are also probably the cause of the small degradation in the tropical winds seen in the case studies. If the temperature and cloud biases could be reduced then it would be reasonable to expect that the tropical winds would also improve. These biases may be addressed by improving the representation of the physical processes rather than via a pure tuning exercise.

The parameter $RDET$ controls the level of adaptivity in the adaptive detrainment (Derbyshire *et al.* (2011)) and plays an important role in determining the vertical structure of convection. A larger value implies a longer tail in the distribution of the buoyancy with respect to the parcel mean buoyancy; this tends to result in a warmer upper tropical troposphere and a cooler lower troposphere as convection is allowed to become deeper. It has been necessary to use a high value of $RDET$ (0.8) in GA7 effectively to compensate for the use of a single compromise entrainment rate. The single entrainment rate is a compromise between having a high value that makes convection more sensitive to humidity and improves variability, and having a low value that allows convection to get sufficiently deep. Within these constraints a large $RDET$ value allows a larger entrainment rate whilst still enabling convection to become sufficiently deep. However, the additional degree of freedom for the entrainment rate with ProgEnt means that the spread of buoyancies can be represented amongst the plumes in a physically sensible manner, rather than being forced to exist within each single plume. It is therefore reasonable and desirable to reduce $RDET$ when using ProgEnt and tests show that this does improve the tropical temperature profile.

As discussed in section 3.1.2 the amount of high-level cloud is reduced by ProgEnt. The amount of total water that the scheme transports to high-levels is dependent not only on the mass flux but also the amount of condensate that the convective parcel can hold before it is converted to precipitation. The amount of condensate that the parcel can hold is controlled by the scheme's "microphysics". Evidence suggests that the amount of in-cloud condensate is too low within the convection scheme and that allowing the parcel to hold more condensate would be a physical improvement. Recent sensitivity tests demonstrate that doing this leads to a beneficial increase in high cloud and improves the tropical temperature profile. Note also that allowing the parcel to hold more condensate will directly reduce precipitation whilst reducing insolation. It is therefore possible that such a change cloud be beneficial to the diurnal cycle although such an effect has not yet been demonstrated.

© Crown Copyright 2017

5 Summary, Conclusion and Future Work

There are numerous problems with the performance of the model in the tropics that are often attributed to the parameterisation of convection. It has been shown that increasing the entrainment rate can improve some aspects of tropical variability, but this degrades the mean climate and NWP performance. It is proposed that tropical variability may be improved without signficantly degrading the mean climate or NWP performance by adding an additional degree of freedom to the entrainment rate controlled by a new prognostic which allows the parameterisation to have ”memory” of recent convective activity. The addition of this prognostic based entrainment rate to the convection scheme is referred to as ProgEnt. This use of convective memory is a first attempt within the UM's convection parameterisation to recognise the fact that (ensembles of) convective clouds develop and grow over a finite timescale, and that the state of convection cannot be uniquely determined from the large-scale state but is also dependent on the subgrid state.

With ProgEnt, memory of recent convective activity is carried within a 3-dimensional prognostic that is advected with the resolved flow and is based on surface convective precipitation. The prognostic uses an empirical e-folding timescale of $\tau = 3\,\mathrm{hours}$; τ is intended to represent the timescale for the mean cloud size within an ensemble of convective clouds including unresolved processes that directly or indirectly affect convective cloud size (e.g. downdraughts and cold pools), but excluding resolved processes that affect convective cloud size. The entrainment rate is related to the prognostic, which is essentially a time-mean precipitation rate, such that if there has been a large amount of recent convective activity a smaller entrainment rate is used, which would imply larger cloud sizes, and if there has been little recent convective activity a larger entrainment rate is used, which would imply smaller cloud sizes. Such a relationship between entrainment and precipitation is shown to be consistent with the behaviour of a simple entraining plume model for idealised tropical and mid-latitude temperature profiles. ProgEnt generates a continuous spectrum of entrainment rates, which is comparable to CRM based estimates, as compared to a single compromise value that is used in the GA7 control. This broadens the spread of convective cloud heights with more convection terminating at low- and mid-levels, whilst still enabling the deepest convection to get deeper.

The impact of ProgEnt on the mean climate in the AMIP simulations is broadly neutral, with only small changes in radiative fluxes and precipitation, but there are increases in the tropical temperature biases with a cooler mid-troposphere and warmer upper troposphere. The NWP case studies show some degradation relative to GA7 . However, this is primarily caused by the same increases in tropical temperature biases and associated circulation changes that can be directly attributed to changes in the convective heating. Therefore, although there are increases in some biases, the changes are well understood and they should be amenable to tuning within the convection scheme. In contrast, HiEnt significantly degrades the mean climate and NWP performance.

One of the goals of convective memory was to improve tropical variability and this is achieved.

© Crown Copyright 2017

The diurnal cycle of precipitation is improved with delays in peak precipitation of 3-4 hours over many, but not all, areas and reductions in the amplitude of the diurnal harmonic. There are beneficial increases to the amount of precipitation during the night over tropical land; this is an indirect effect because mid-level convection, which provides almost all overnight convection, is unchanged by ProgEnt. ProgEnt produces spatially more coherent convection and beneficially increases the peak precipitation rates in the tropics; consequently convective precipitation looks more realistic than in the control. The number and strength of AEWs is beneficially increased whilst the impact on equatorial waves and the MJO is small.

We have shown that ProgEnt is able to improve some aspects of tropical variability, i.e. the diurnal cycle and precipitation intensity, whilst maintaining, or in some cases improving, the mean climate and NWP performance. It is able to do this because the additional degree of freedom given to the entrainment rate allows it to vary within a realistic range of values. Simply increasing the entrainment rate does improve the diurnal cycle but the depth of the deepest tropical convection is detrimentally reduced and the tropical circulation is consequentially degraded. Using a single entrainment rate is inevitably a compromise between capturing the mean state and capturing the variability. ProgEnt avoids the need to make this compromise.

If a sufficient level of performance can be achieved when it is packaged with other changes then it is intended that ProgEnt will be included in the next global atmosphere configuration, GA8. Such a package may include changes to the convective cloud and to the adaptive detrainment. Further exploration of ProgEnt's parameter space may yield further improvements in performance.

Future improvements to ProgEnt will include its extension to mid-level convection. This already technically works. Mid-level convection, however, is currently given a very small initial perturbation and this will need to be revised to avoid it being over suppressed when combined with an entrainment rate that will often be much higher than its current fixed value. Such developments to the mid-level scheme would reduce the distinction between mid-level and deep convection and raises the possibility of combining them both into a single scheme. Furthermore, having a single convection type that may have a wide range of entrainment rates raises the possibility of also eliminating the need for separate shallow and deep schemes: this would be particularly attractive as it would also remove the need to diagnose which type of convection is active, which is a process that inevitably involves arbitrary thresholds. Ultimately, ProgEnt and, in a more general sense, convective "memory" could allow the use of a single convection scheme that adapts to its environment and allows convection to develop in a realistic manner.

The use of "memory" within the convection could be extended to include other aspects of subgrid variability and in particular the initial perturbation that is applied to the convective parcel. Sensitivity tests have been performed in which the parcel kinetic energy and buoyancy perturbations (used in the convective diagnosis to determine whether a lifted parcel may overcome the Convective Inhibition (CIN) and trigger convection) include a contribution from the convective prognostic field $\bar{P}$. Combined with ProgEnt, this leads to a significant further increase in the organisation of param-

© Crown Copyright 2017

eterised convection in the Tropics. Since regions of active convection can then trigger convection under a higher-CIN environment, the Tropical mean profiles equilibrate with higher CIN, which suppresses convection outside the most active areas. Areas of active convection therefore become more persistant and more confined, as observed. This lends support to the idea that convective variability in the global UM could be further improved by the inclusion of a prognostic representation of convective cold-pools and their effect on convective triggering. Such a scheme is being developed, and will be reported elsewhere.

6 Acknowledgements

The authors are grateful to Sean Milton, the members of the Convection and Global Model Evaluation and Development groups at the Met Office, and to the Tropical Convection working group for all their helpful comments.

© Crown Copyright 2017

References

Bechtold, P., Kohler, M., Jung, T., Francisco, D.-R., Leutbecher, M., Rodwell, M. J., Vitart, F., and Balsamo, G. 2008. Advances in simulating atmospheric variability with the ECMWF model: From synoptic to decadal time-scales. *Q. J. R. Meteorol. Soc.* **134**: 1337–1351.

Bechtold, P., Semane, N., Lopez, P., Chaboureau, J.-P., Beljaars, A., and Bormann, N. 2014. Representing Equilibrium and Nonequilibrium Convection in Large-Scale Models. *J. Atmos. Sci.* **74**: 734–753.

Bush, S. J., Turner, A. G., Woolnough, S. J., Martin, G. M., and Klingaman, N. 2015. The effect of increased convective entrainment on Asian monsoon biases in the MetUM general circulation model. *Q. J. R. Meteorol. Soc.* **141**: 311–326.

Davies, L., Plant, R., and Derbyshire, S. H. 2009. A simple model of convection with memory. *J. Geophys. Res.* **114**.

Davies, L., Plant, R. S., and Derbyshire, S. H. 2013. Departures from convective equilibrium with a rapidly varying surface forcing. *Q. J. R. Meteorol. Soc.* **139**: 1731–1746.

de Rooy, W. C., Bechtold, P., Frohlich, K., Hohenegger, C., Jonker, H., Mironov, D., Siebesma, A. P., Teixeira, J., and Yano, J.-I. 2013. Entrainment and detrainment in cumulus convection: an overview. *Q. J. R. Meteorol. Soc.* **139**: 1–19.

Del Genio, A. D. and Jingbo, W. 2009. The Role of Entrainment in the Diurnal Cycle of Continental Convection. *J. Clim.* **23**: 2722–2738.

Derbyshire, S. H., Maidens, A. V., Milton, S. F., Stratton, R. A., and Willett, M. R. 2011. Adaptive detrainment in a convection parametization. *Q. J. R. Meteorol. Soc.* **137**(660): 1856–1871.

Gregory, D. and Rowntree, P. R. 1990. A mass flux convection scheme with representation of cloud ensemble characteristics and stability dependent closure. *Mon. Wea. Rev.* **118**: 1483–1506.

Hardiman, S. C., Boutle, I. A., Bushell, A. C., Butchart, N., Cullen, M. J. P., Field, P. R., Furtado, K., Manners, J. C., Milton, S. F., Morcrette, C., O'Connor, F. M., Shipway, B. J., Smith, C., Walters, D. N., Willett, M. R., Williams, K. D., Wood, N., Abraham, N. L., Keeble, J., Maycock, A. C., Thuburn, J., and Woodhouse, M. T. 2015. Processes Controlling Tropical Tropopause Temperature and Stratospheric Water Vapor in Climate Models. *J. Clim.* **28**: 6516–6535.

Hohenegger, C. and Bretherton, C. S. 2011. Simulating deep convection with a shallow convection scheme. *Atmos. Chem. Phys.* **11**: 10389–10406.

Hohenegger, C. and Stevens, B. 2012. Preconditioning Deep Convection with Cumulus Congestus. *J. Atmos. Sci.* **70**: 448–464.

© Crown Copyright 2017

Houze Jr, R. A. 2004. Mesoscale Convective Systems. *Rev. Geophys.* **42**(RG4003).

Huffman, G., Adler, R., Bolvin, D., Gu, G., Nelkin, E., Bowman, K., Hong, Y., Stocker, E., and Wolff, D. 2007. The TRMM Multi-satellite Precipitation Analysis: Quasi-Global, Multi-Year, Combined-Sensor Precipitation Estimates at Fine Scale. *J. Hydrometeor.* **8**: 38–55.

Kain, J. S. 2004. The Kain-Fritsch Convective Parameterization: An Update. *J. App. Met.* **43**: 170–181.

Klingaman, N. and Woolnough, S. 2014. Using a case-study approach to improve the Madden Julian oscillation in the Hadley Centre model. *Q. J. R. Meteorol. Soc.* **141**: 2491–2505.

Machado, L. A. T., Rossow, W. B., Guedes, R. L., and Walker, A. W. 1998. Life Cycle Variations of Mesoscale Convective Systems over the Americas. *Mon. Wea. Rev.* **126**: 1630–1654.

Mapes, B. and Neale, R. 2011. Parameterizing Convective Organization to Escape the Entrainment Dilemma. *J. Adv. Model. Earth Syst.* **3**.

Martin, G. M., Klingaman, N. P., and Moise, A. F. 2017. Connecting spatial and temporal scales of tropical precipitation in observations and the MetUM-GA6. *Geosci. Model Dev.* **10**.

Met Office 1996. *Source book to the Forecasters' Reference Book*. Exeter, UK.

Piriou, J.-M., Redelsperger, J.-L., Geleyn, J.-F., Lafore, J.-P., and Guichard, F. 2007. An Approach for Convective Parameterization with Memory: Separating Microphysics and Transport in Grid-Scale Equations. *J. Atmos. Sci.* **64**: 4127–4139.

Simpson, J. and Wiggert, V. 1965. Models of precipitating cumulus towers. *Mon. Wea. Rev.* **4**(4): 471–489.

Stirling, A. J. and Stratton, R. A. 2011. Entrainment processes in the diurnal cycle of deep convection. *Q. J. R. Meteorol. Soc.*

Stratton, R. A. and Stirling, A. J. 2011. Improving the diurnal cycle of convection in gcms. *Q. J. R. Meteorol. Soc.*

Walters, D. N., Brooks, M., Boutle, I., Melvin, T., Stratton, R., Vosper, S., Wells, H., Williams, K., Wood, N., Allen, T., Bushell, A., Copsey, D., Earnshaw, P., Edwards, J., Gross, M., Hardiman, S., Harris, C., Heming, J., Klingman, N., Levine, R., Manners, J., Martin, G., Milton, S., Mittermaier, M., Morcrette, C., Riddick, T., Roberts, M., Sanchez, C., Selwood, P., Stirling, A., Smith, C., Suri, D., Tennant, W., Vidale, P. L., Wilkinson, J., Willett, M., Woolnough, S., and Xavier, P. 2016. The Met Office Unified Model Global Atmosphere 6.0/6.1 and JULES Global Land 6.0/6.1 configurations. *Geosci. Model Dev.* **4**: 919–941.

© Crown Copyright 2017

Willett, M. R., Bechtold, P., Williamson, D. L., Petch, J. C., Milton, S. F., and Woolnough, S. J. 2008. Modelling suppressed and active convection. Comparisons between three global atmospheric models. *Q. J. R. Meteorol. Soc.* **134**: 1881–1896.

Wilson, J. W., Crook, N. A., Mueller, C. K., Sun, J., and Dixon, M. 1998. Nowcasting Thunderstorms: A Status Report. *Bull. Amer. Meteor. Soc.* **79**(10): 2079–2099.

© Crown Copyright 2017

7 Figures

List of Figures

1 Entrainment profiles . . . 26
2 3-hour-mean convective precipitation rate and $\bar{P}$ for Africa and the Tropical Atlantic. 27
3 As for Figure 2 but for the West Pacific, South-East Asia and Australia . . . 28
4 Precipitation rate as a function of entrainment rate . . . 29
5 Histogram of entrainment rates . . . 30
6 Time-height profiles of entrainment rate . . . 31
7 Frequency of termination level for deep convection . . . 32
8 Deep and total convective mass flux flux . . . 32
9 Profiles of cloud frequency . . . 33
10 Temperature increments from day one . . . 34
11 Temperature increments from day five . . . 34
12 Humidity increments from day one . . . 35
13 Humidity increments from day five . . . 35
14 Cloud condensate increments from day one . . . 36
15 Cloud condensate increments from day five . . . 36
16 Zonal mean temperture . . . 37
17 Temperature spinup . . . 38
18 Convective mass flux spinup . . . 39
19 Precipitation rates for the West Pacific, South-East Asia and Australia . . . 40
20 Precipitation rates for Africa and the Tropical Atlantic . . . 41
21 Spectra of the precipitation rate weighted frequency of 3-hourly total precipitation rate 42
22 Hovmoller of precipitation from TRMM . . . 42
23 Hovmoller from GA7 . . . 43
24 Hovmoller from ProgEnt . . . 44
25 Seasonal mean diurnal cycle of total precipitation . . . 45
26 African easterly wave summary . . . 46
27 Annual mean precipitation . . . 47
28 Annual mean outgoing SW . . . 48
29 Annual mean OLR . . . 49
30 Global troposphere metrics plot . . . 50
31 Global index impact for ProgEnt . . . 51
32 Global index impact for HiEnt . . . 51
33 Case study verification of tropical 850 hPa winds . . . 52
34 Case study verification of tropical 250 hPa winds . . . 52

© Crown Copyright 2017

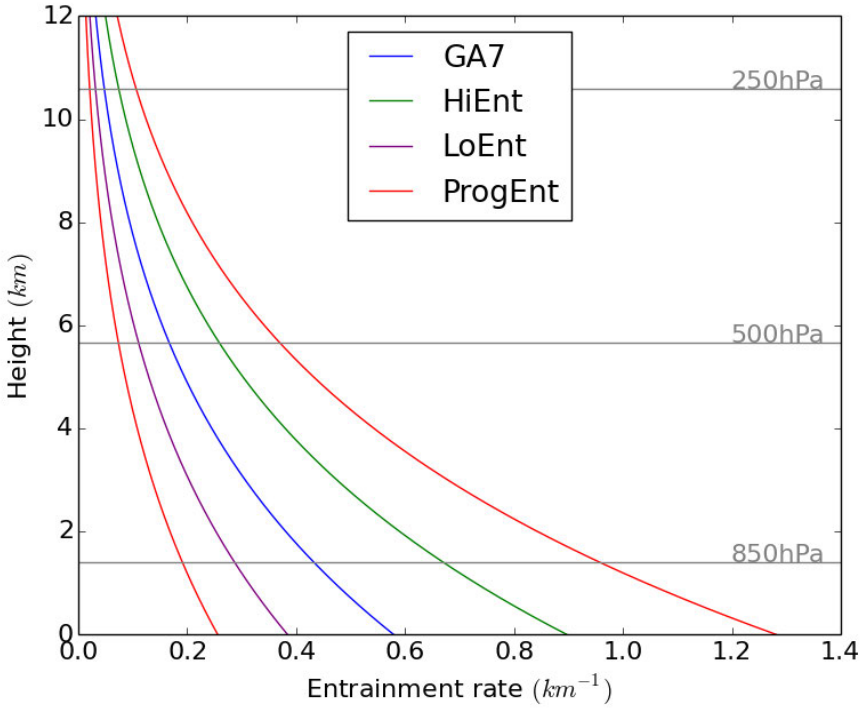

Figure 1: Entrainment profiles in km^{-1} from GA7 (blue), HiEnt (green), LoEnt (purple) and the minimum and maximum values from ProgEnt (red). The entrainment rates have been converted from Pa^{-1}, which is used internally within the convection scheme, to km^{-1} assuming a constant $7\,\mathrm{Kkm}^{-1}$ lapse rate.

© Crown Copyright 2017

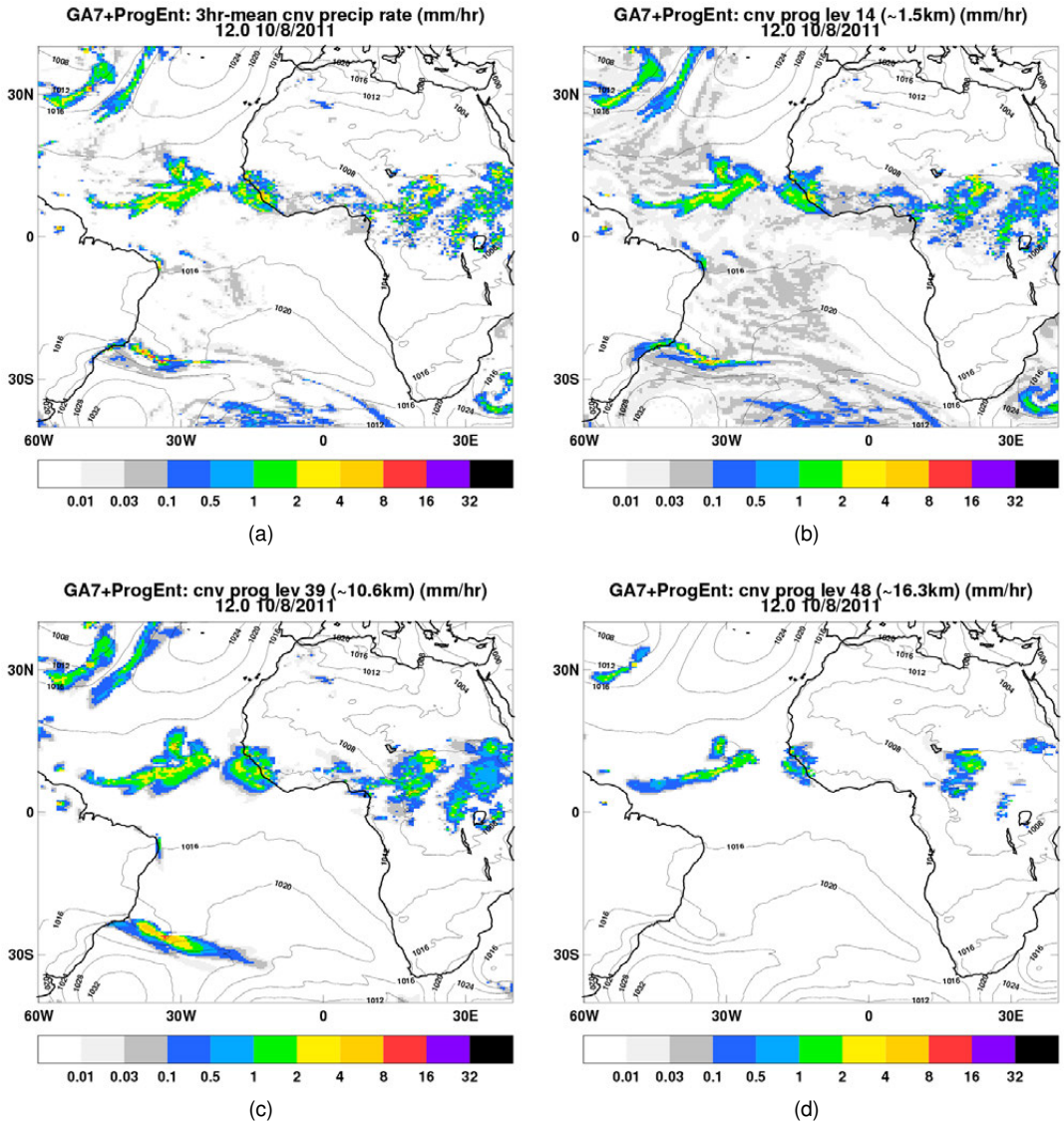

Figure 2: On the colour-scale (in mm hour^{-1}): (a) 3-hour-mean convective precipitation rate and $\bar{P}$ from (b) model level 14 ($\approx 1.5\,\mathrm{km}$), (c) model level 39 ($\approx 10.6\,\mathrm{km}$) and (d) model level 48 ($\approx 16.3\,\mathrm{km}$) at T+36 from a ProgEnt N320 case study for Africa and the Tropical Atlantic. The surface pressure is also contoured in black on each panel.

© Crown Copyright 2017

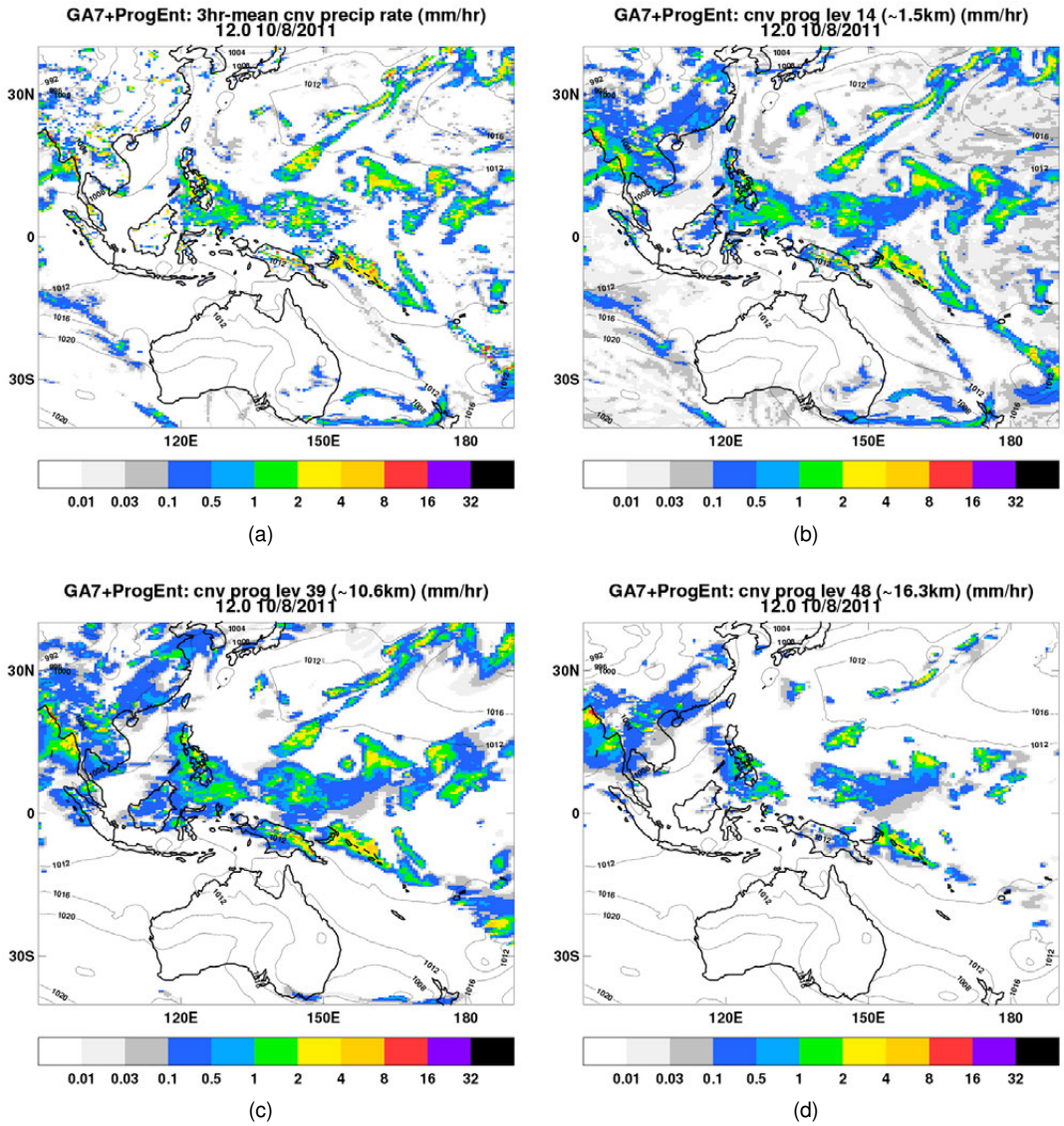

Figure 3: As for Figure 2 but for the West Pacific, South-East Asia and Australia

© Crown Copyright 2017

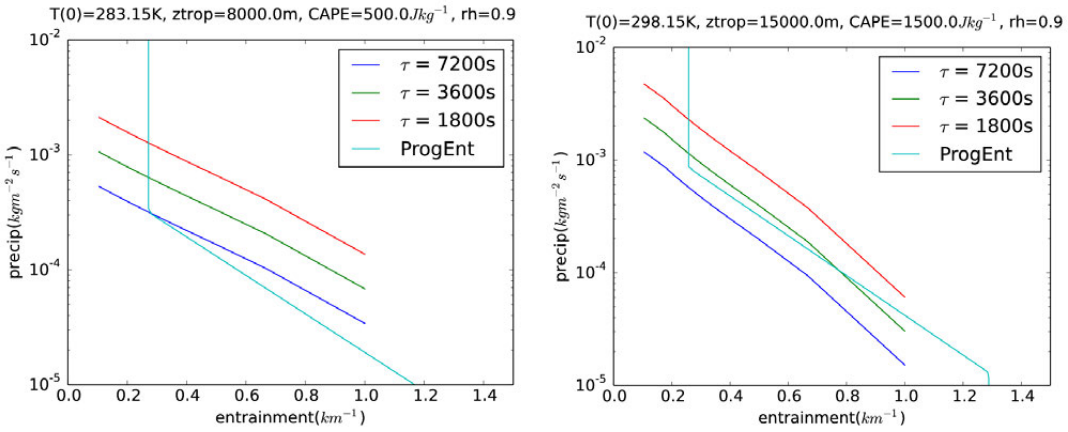

Figure 4: Precipitation rate as a function of entrainment rate for idealised (a) midlatitude and (b) tropical atmospheric profiles, from a simple plume model with CAPE timescales of 2 hours (blue), 1 hour (green), 30 minutes (red) and the prognostic entrainment relationship in eq (3) (light blue).

© Crown Copyright 2017

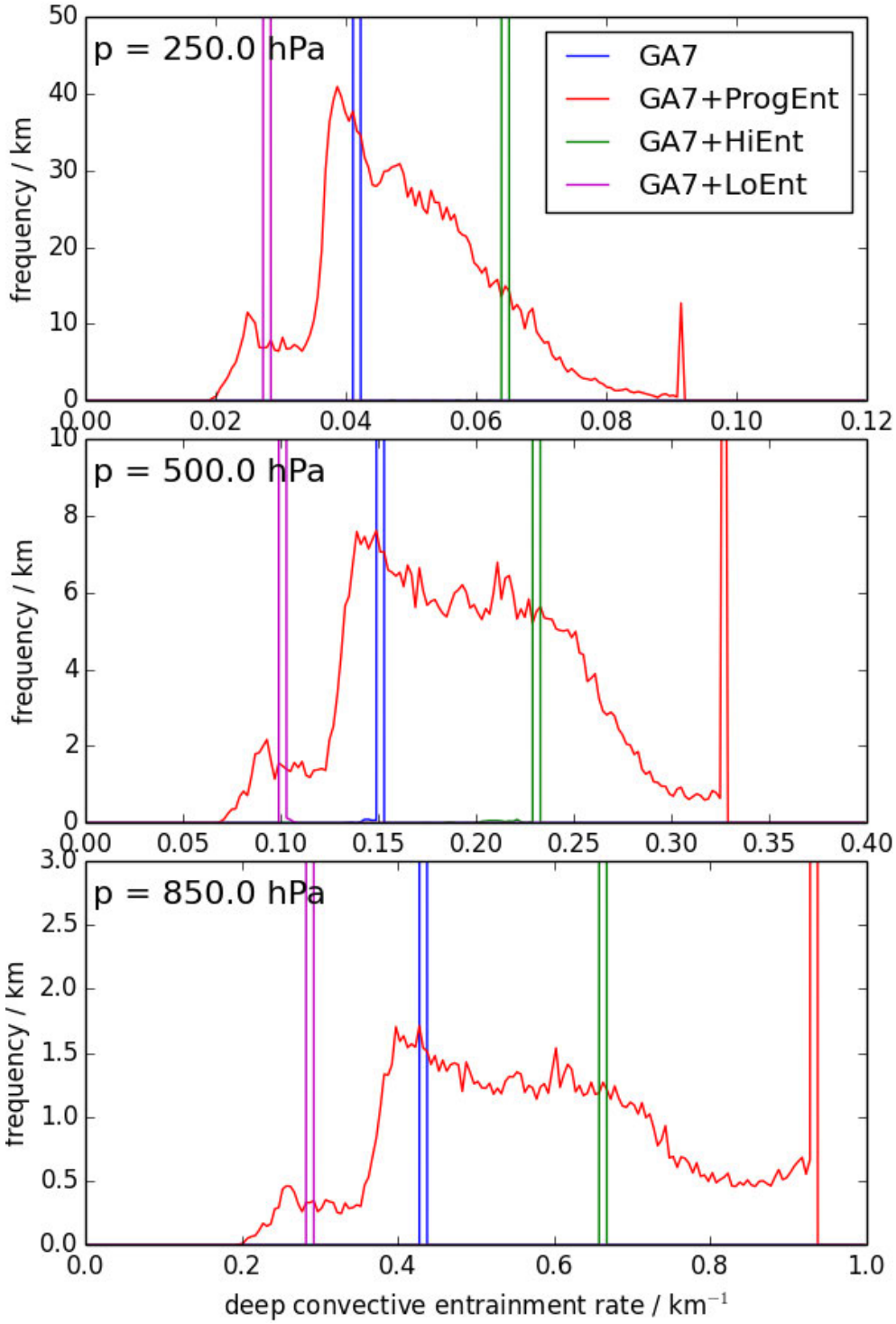

Figure 5: Histogram of entrainment rates in the main ascent from an ensemble of SCM simulations of Toga-Coare at $250\,\mathrm{hPa}$ (top), $500\,\mathrm{hPa}$ (middle), and $850\,\mathrm{hPa}$ (bottom). Rates are from GA7 (blue), ProgEnt (red), HiEnt (green) and LoEnt (magenta). Note that the range of entrainment rates on the x-axis varies with height.

© Crown Copyright 2017

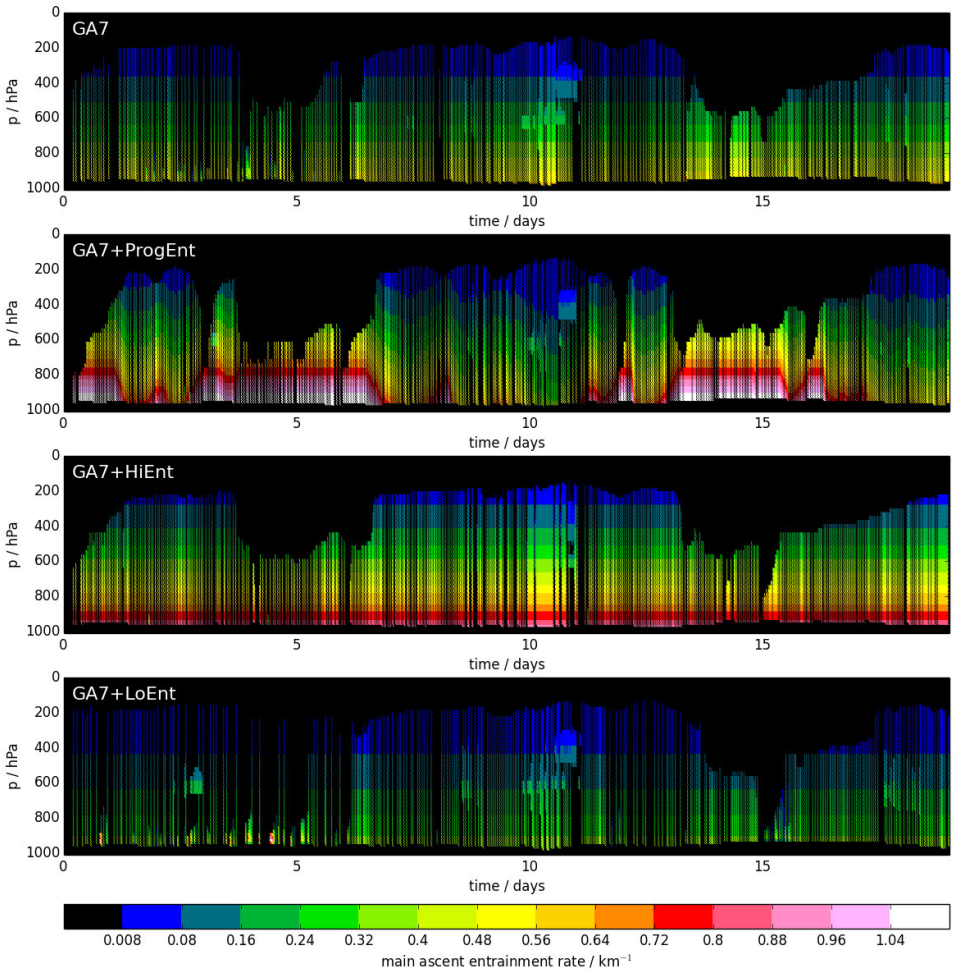

Figure 6: Time-height profiles of entrainment rate from SCM simulations of Toga-Coare showing from the top GA7, ProgEnt, HiEnt and LoEnt.

© Crown Copyright 2017

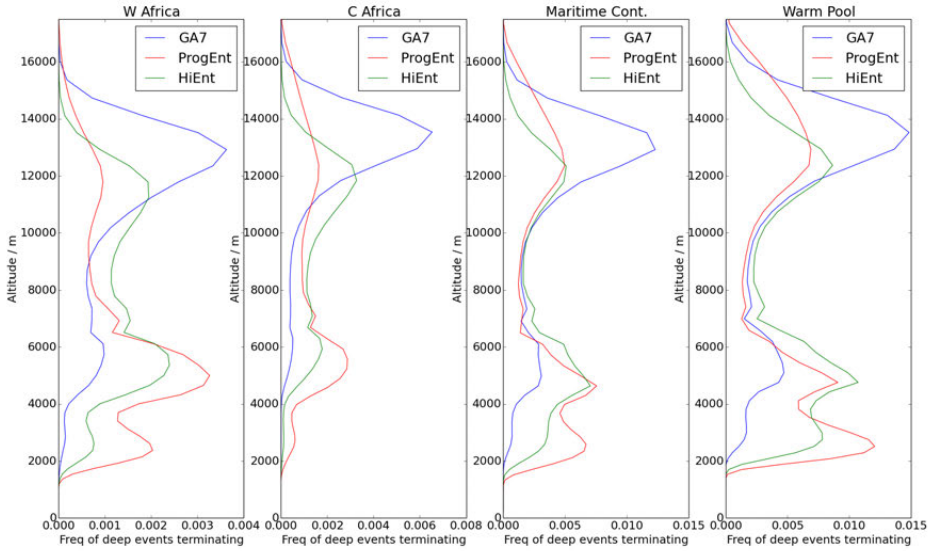

Figure 7: Frequency of termination level for deep convection from GA7 (blue), ProgEnt (red) and HiEnt (green) for West Africa, Central Africa, Maritime Continent and the West Pacific warm pool from 20 year AMIP simulations.

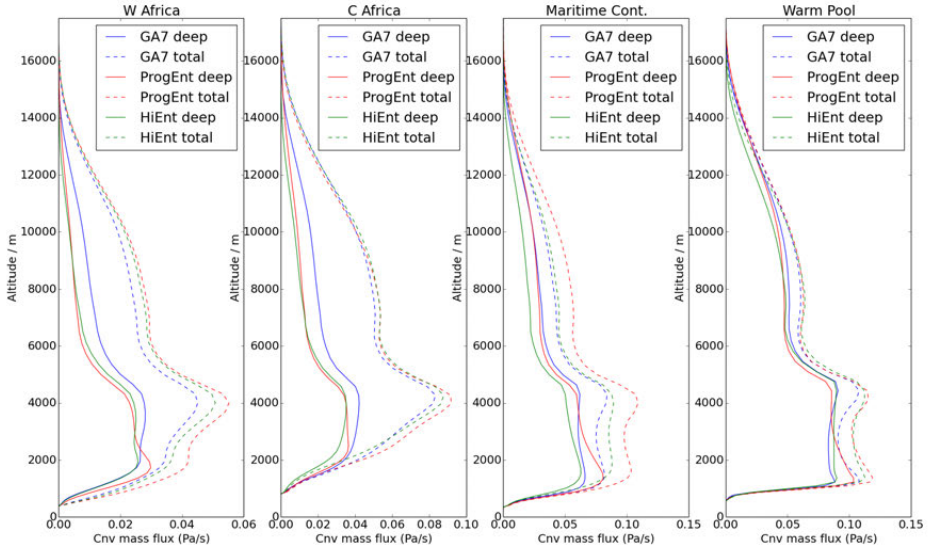

Figure 8: Deep convective mass flux (solid) and total convective mass flux (dashed) from GA7 (blue), ProgEnt (red) and HiEnt (green) for West Africa, Central Africa, Maritime Continent and the West Pacific warm pool from 20 year AMIP simulations.

© Crown Copyright 2017

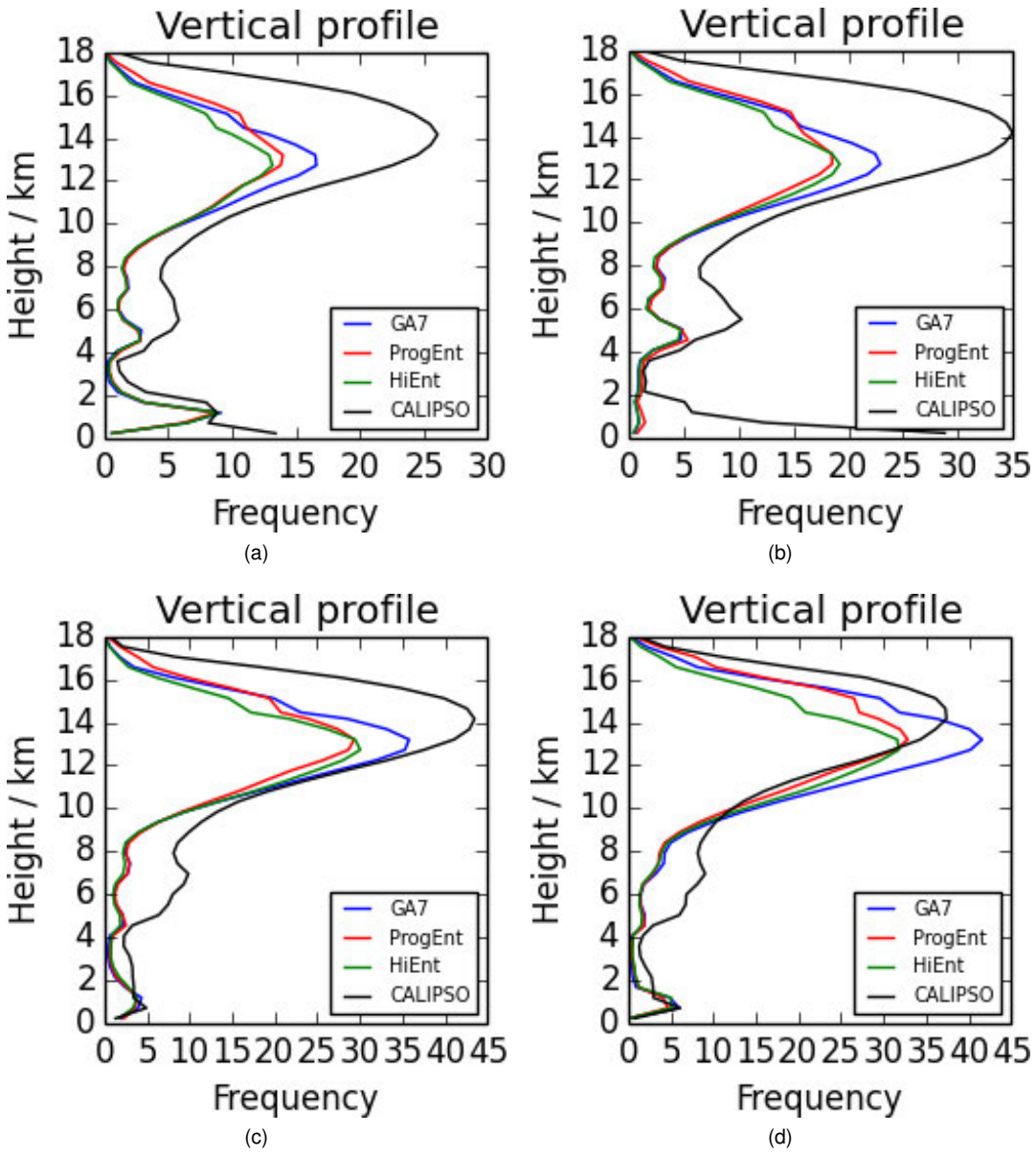

Figure 9: Profiles of cloud frequency formed by integrating across all backscatter ratios from CALIPSO observations (black) and from the CALIPSO simulator applied to 20-year AMIP simulations of GA7 (blue), ProgEnt (red) and HiEnt (green) for (a) West Africa, (b) Central Africa, (c) Maritime Continent and (d) West Pacific warm pool.

© Crown Copyright 2017

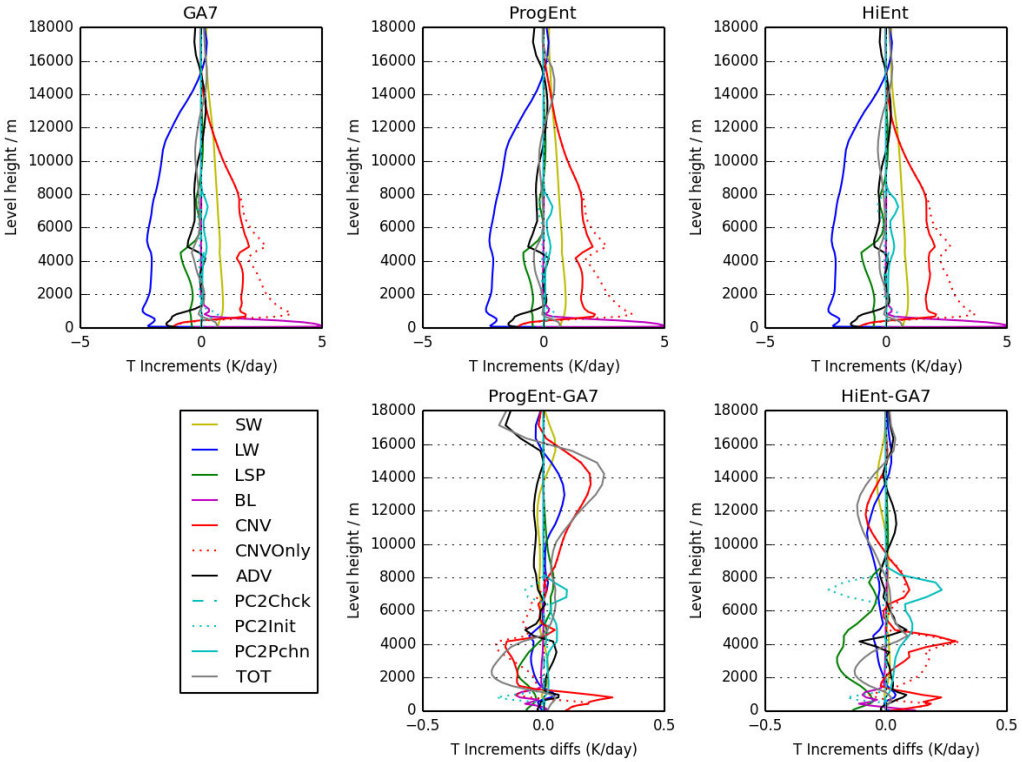

Figure 10: Temperature increment profiles for the tropics (20S-20N) from day one of the case studies from GA7 (top left), ProgEnt (top middle), HiEnt (top right), ProgEnt-GA7 (bottom middle) and HiEnt-GA7 (bottom right).

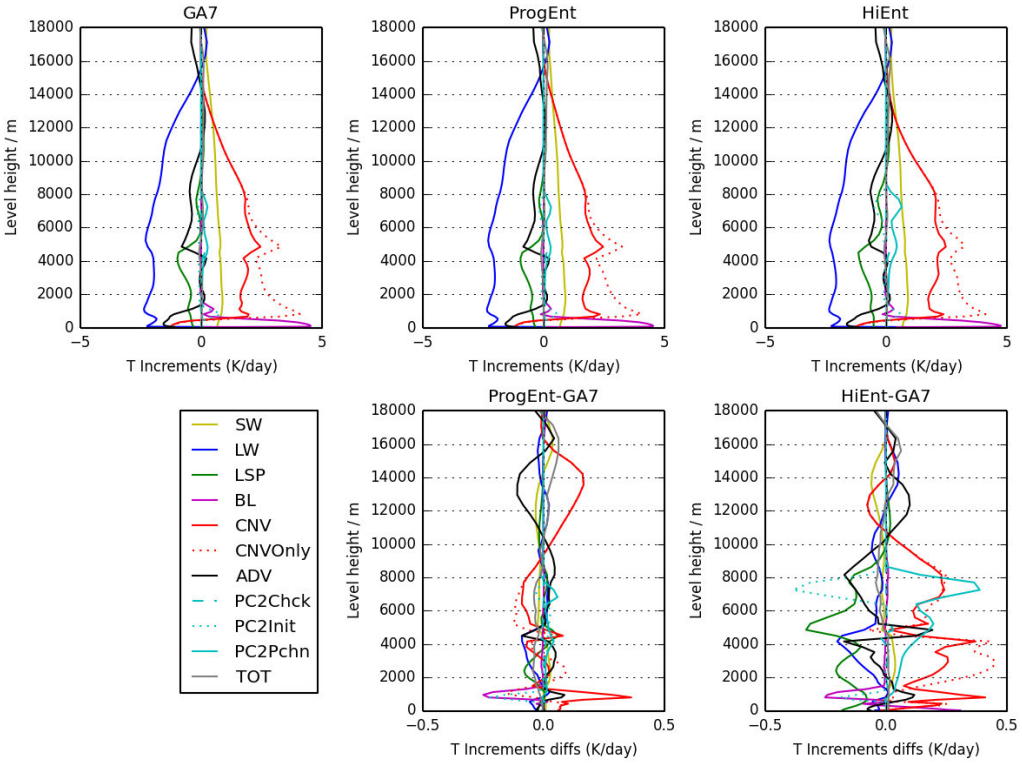

Figure 11: As figure 10 but for day five.

© Crown Copyright 2017

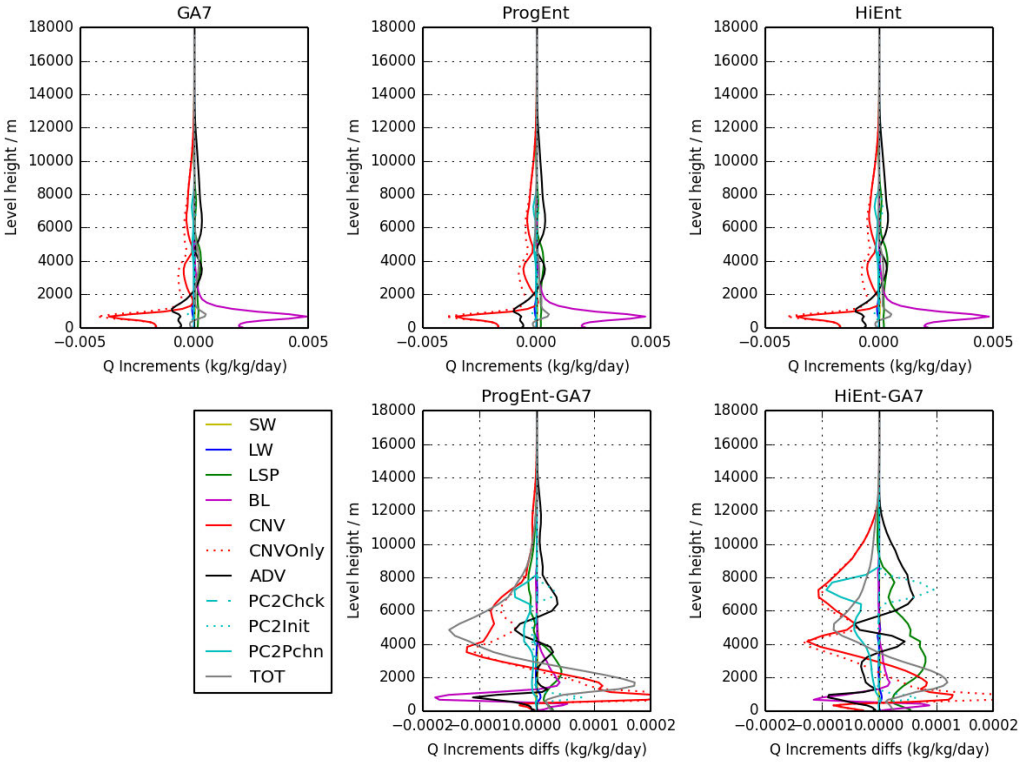

Figure 12: Specific humidity increment profiles for the tropics (20S-20N) from day one of the case studies from GA7 (top left), ProgEnt (top middle), HiEnt (top right), ProgEnt-GA7 (bottom middle) and HiEnt-GA7 (bottom right).

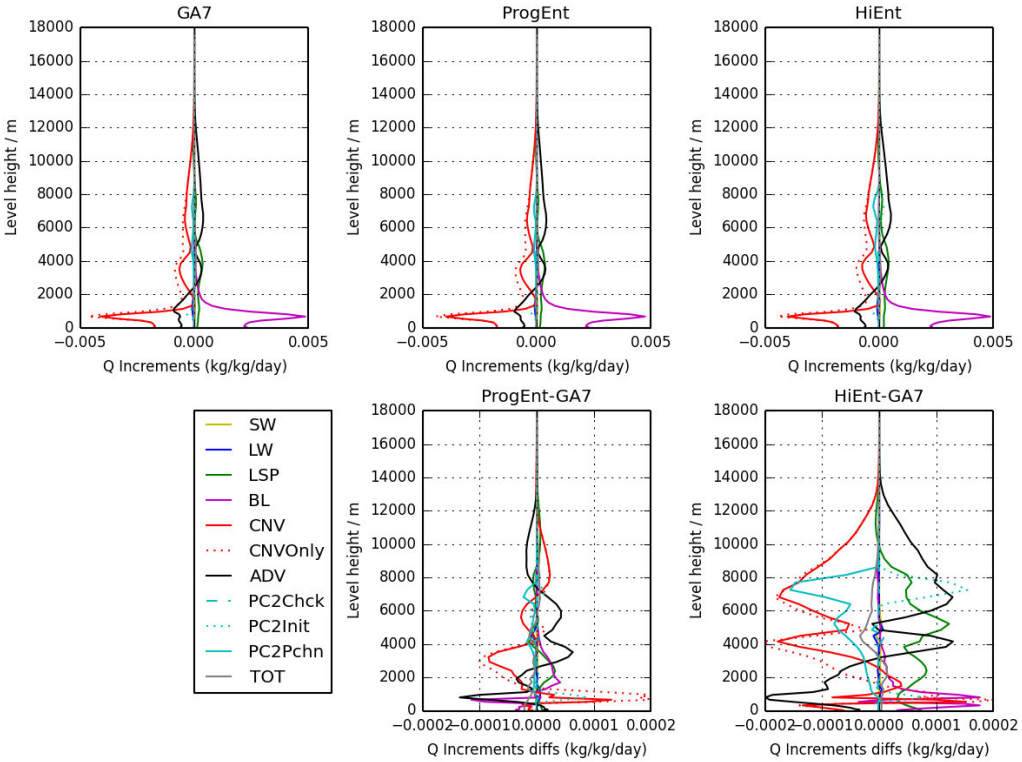

Figure 13: As figure 12 but for day five.

© Crown Copyright 2017

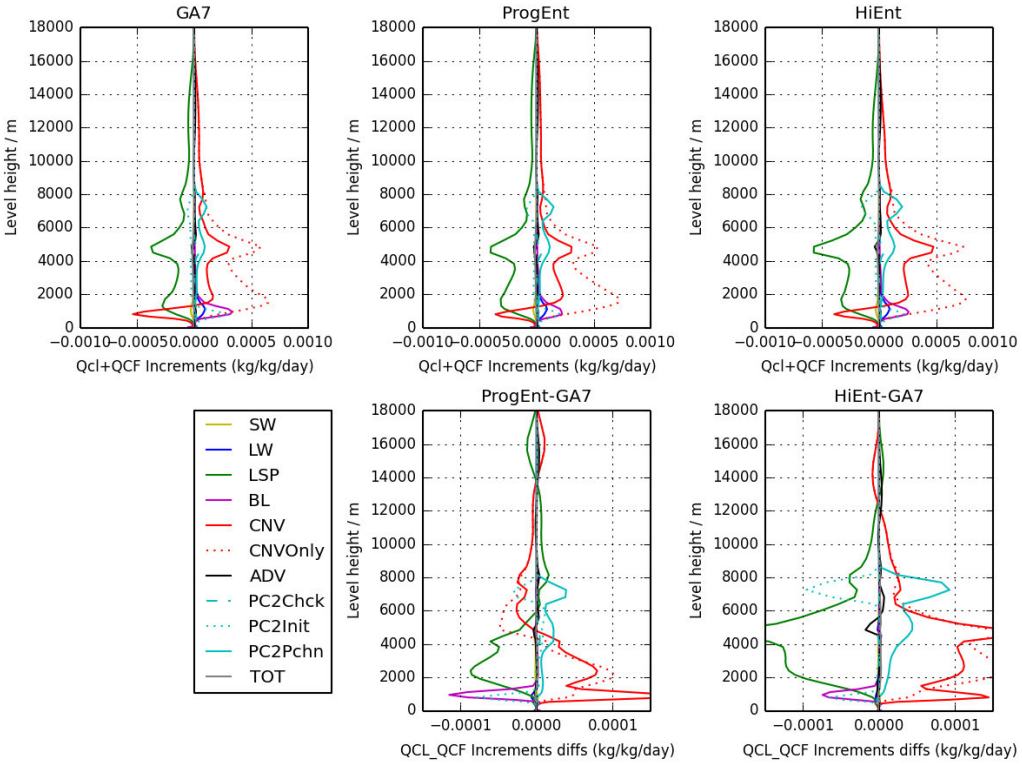

Figure 14: Cloud condensate increment profiles for the tropics (20S-20N) from day one of the case studies from GA7 (top left), ProgEnt (top middle), HiEnt (top right), ProgEnt-GA7 (bottom middle) and HiEnt-GA7 (bottom right).

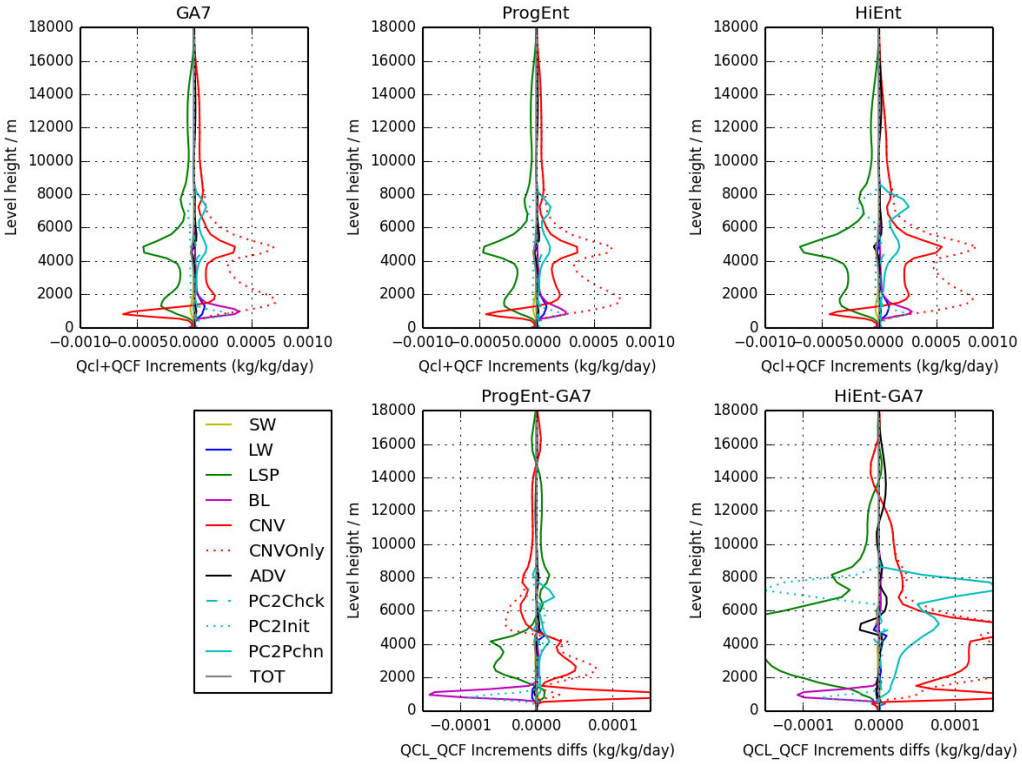

Figure 15: As figure 14 but for day five.

© Crown Copyright 2017

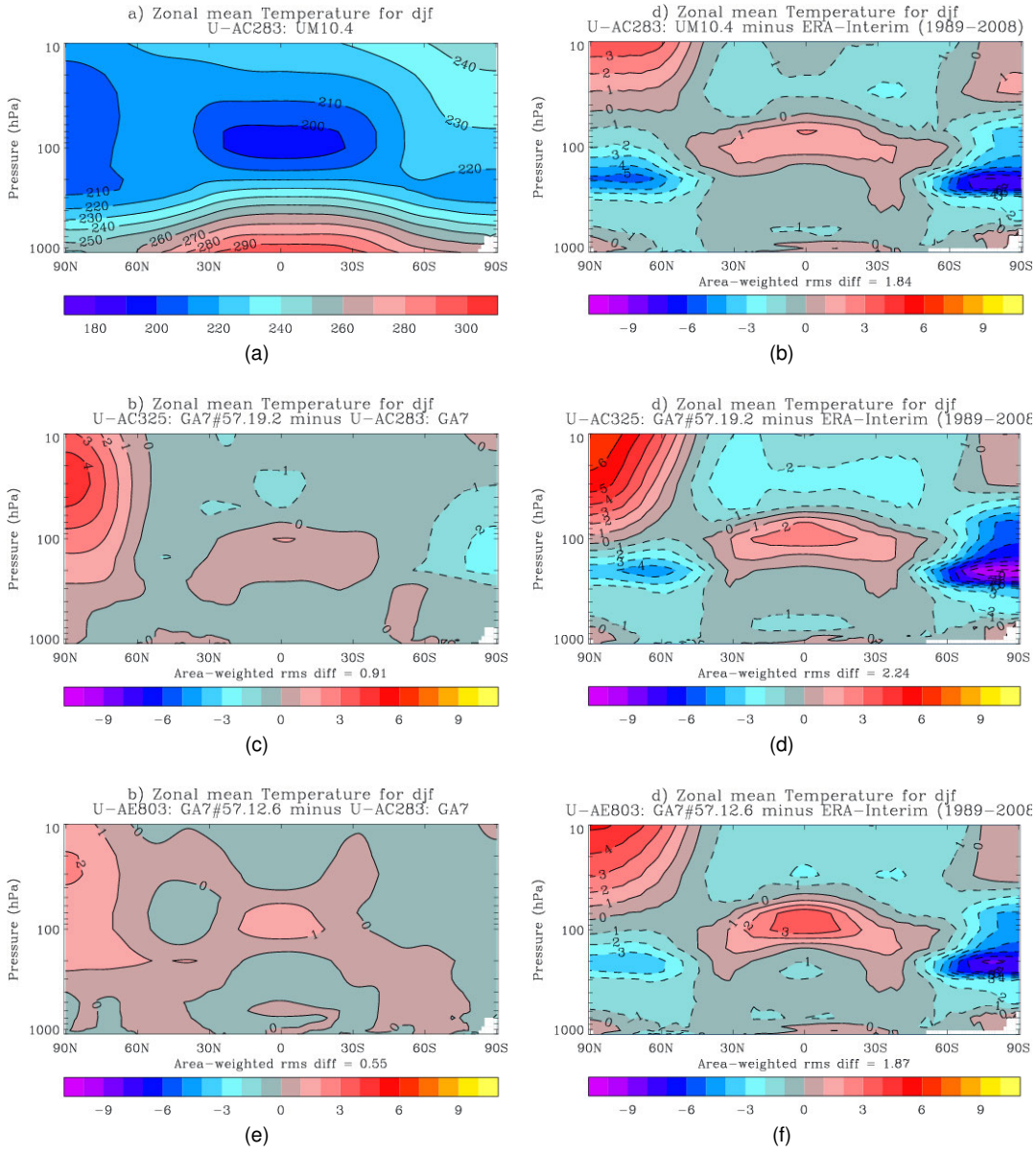

Figure 16: Zonal mean temperture for DJF in the 20 yr N96 simulations: (a) GA7, (b) GA7-ERAI, (c) ProgEnt-GA7, (d) ProgEnt-ERAI, (e) HiEnt-GA7 and (f) HiEnt-ERAI.

© Crown Copyright 2017

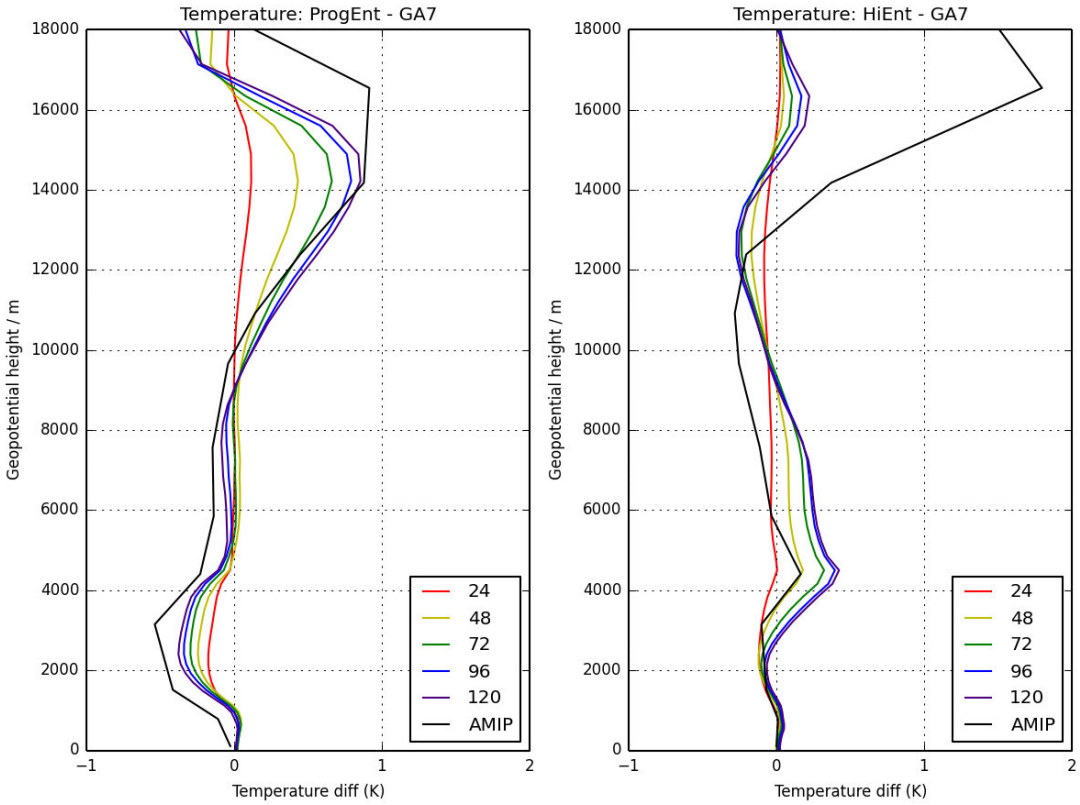

Figure 17: Profiles showing the spin-up of temperature relative to GA7 for ProgEnt (left) and HiEnt (right).

© Crown Copyright 2017

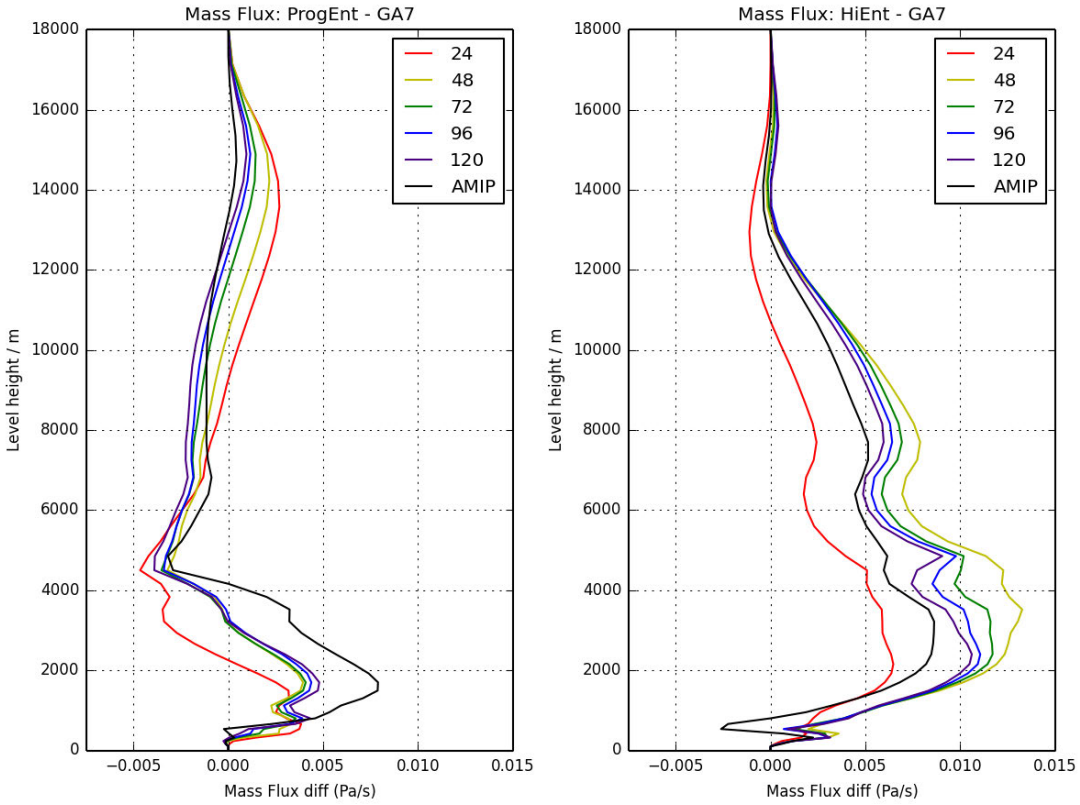

Figure 18: Profiles showing the spin-up of total convective mass flux relative to GA7 for ProgEnt (left) and HiEnt (right).

© Crown Copyright 2017

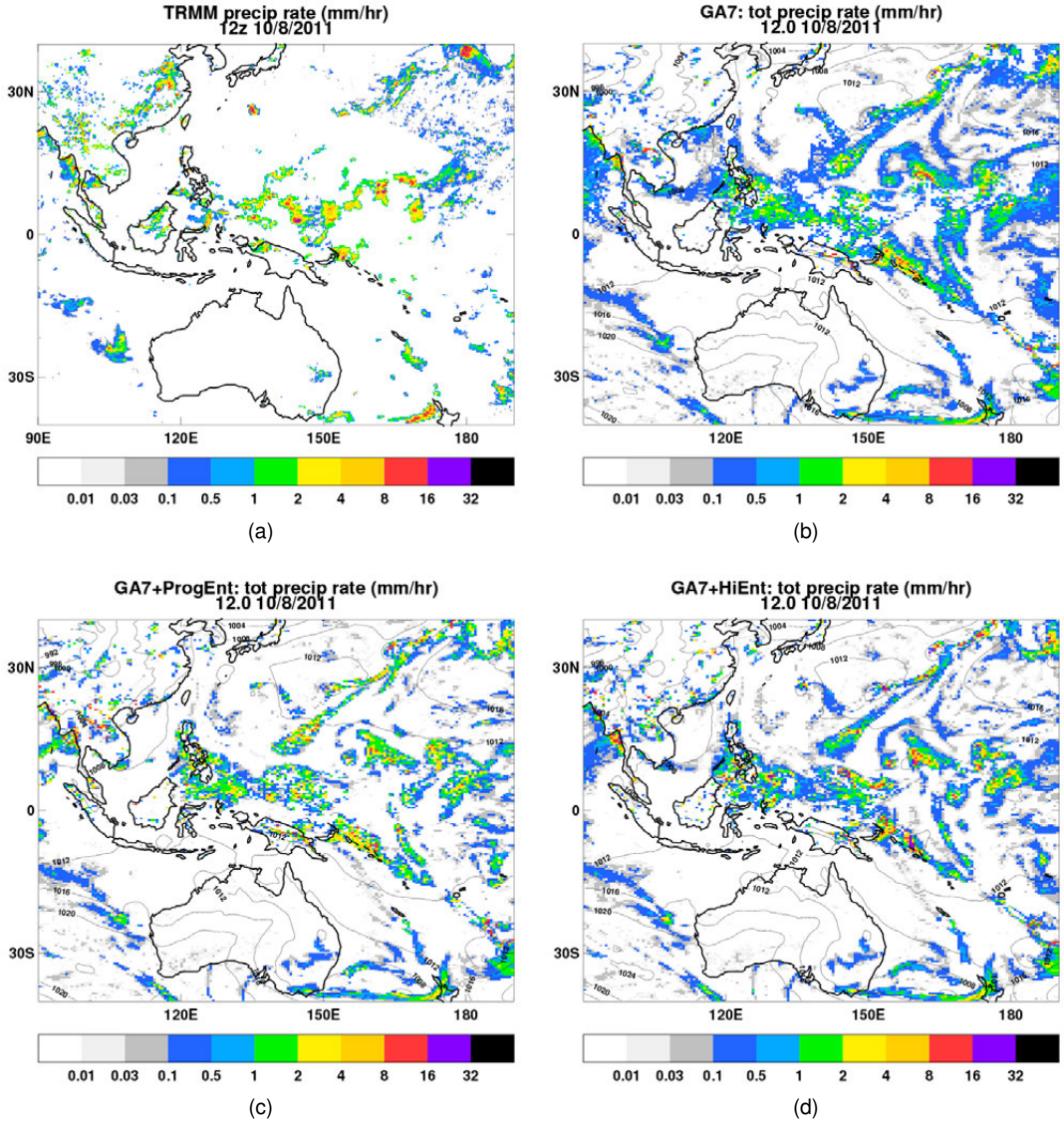

Figure 19: Precipitation rate from (a) TRMM, and T+36 forecasts from (b) GA7, (c) ProgEnt and (d) HiEnt for the West Pacific, South-East Asia and Australia

© Crown Copyright 2017

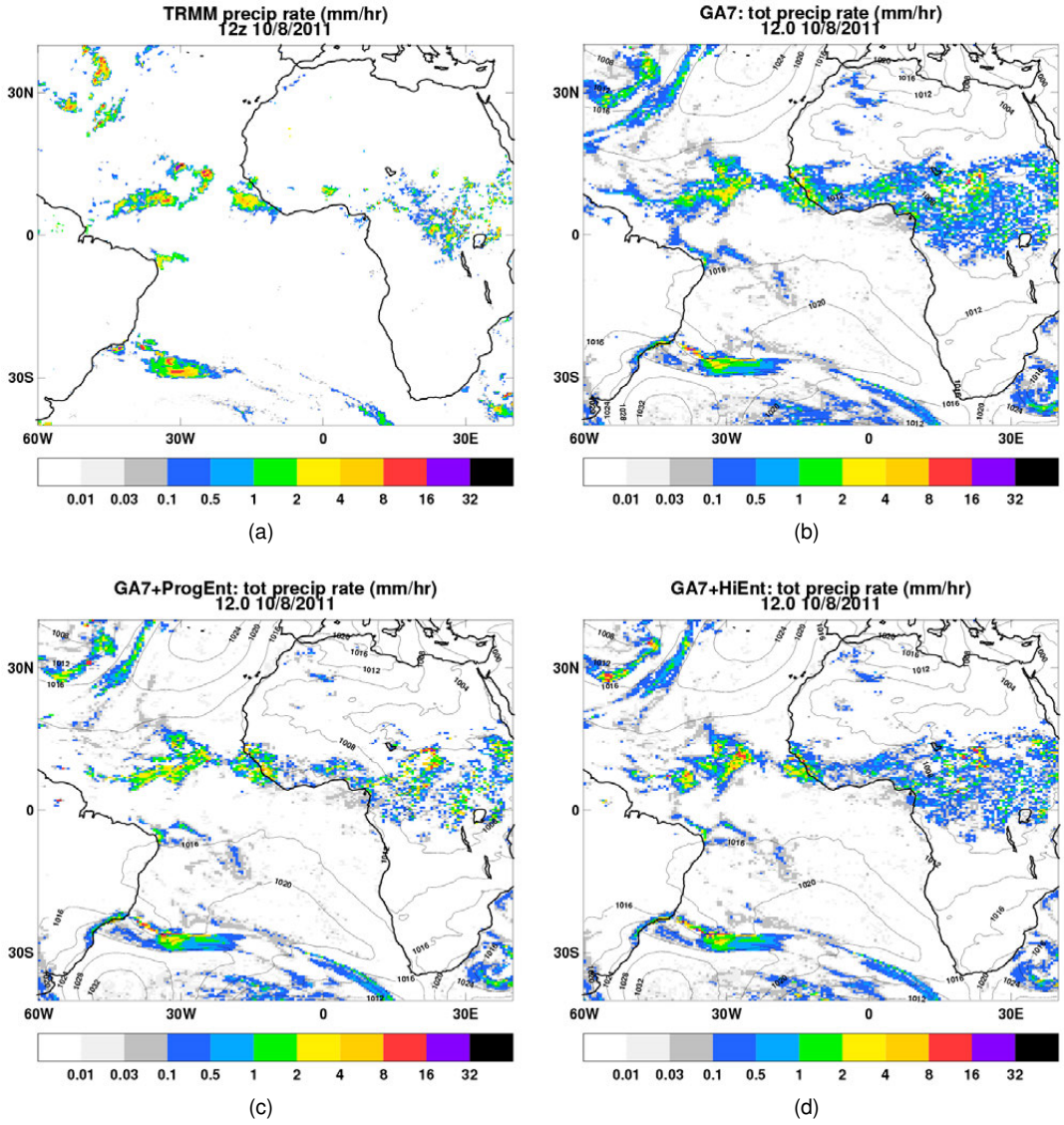

Figure 20: Precipitation rate from (a) TRMM, and T+36 forecasts from (b) GA7, (c) ProgEnt and (d) HiEnt for Africa and the Tropical Atlantic.

© Crown Copyright 2017

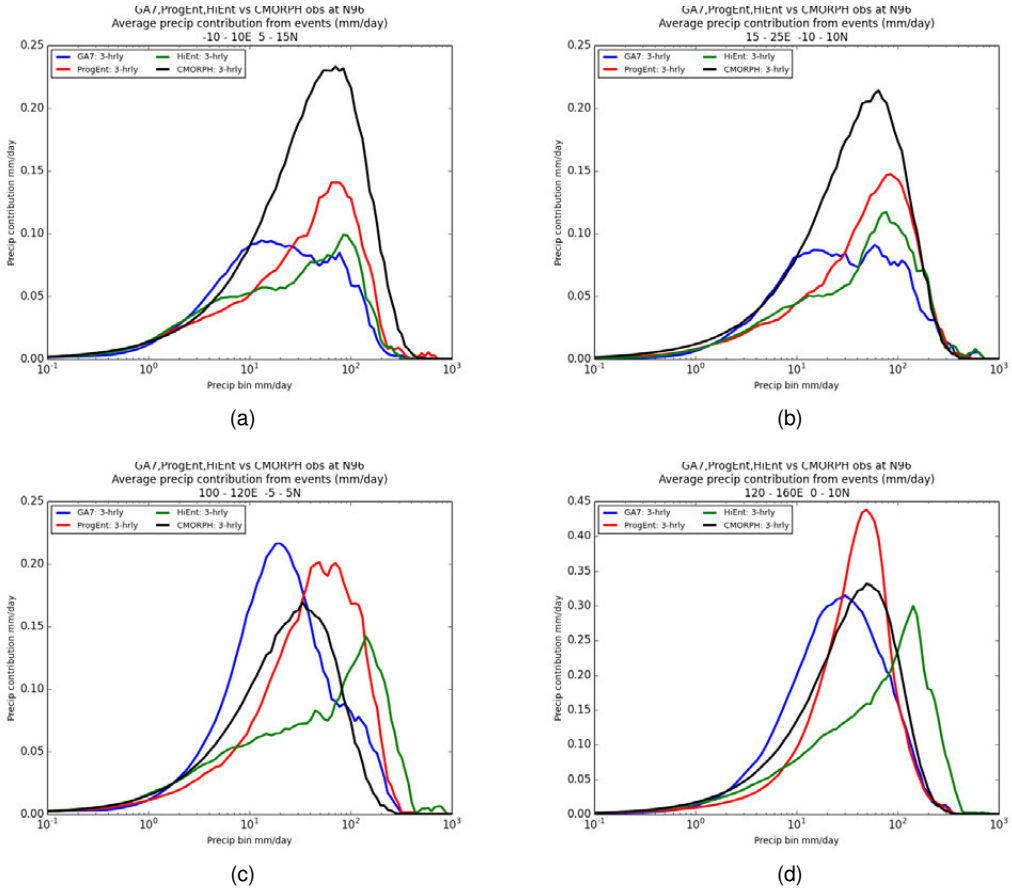

Figure 21: Spectra of the precipitation weighted frequency of 3-hourly total precipitation rate for (a) West Africa, (b) Central Africa, (c) Maritime Continent and (d) West Pacific warm pool from CMORPH (black) and from 4-months of the AMIP simulations using GA7 (blue), ProgEnt (red) and HiEnt (green). The precipitation weighted frequency is defined as $p_i \frac{n_i}{N}$ where p_i is the precipitation rate at the centre of bin i, n_i is the number of events in the bin i and N is the total number of events. The integral under each curve is equal to the total precipitation rate but note the logarithmic x-axis.

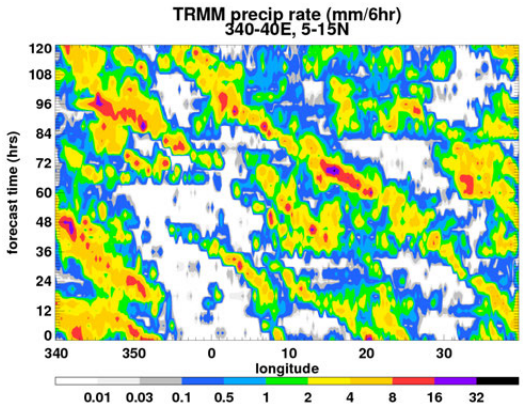

Figure 22: Hovmoller of precipitation from TRMM showing east-west section of Africa from the Atlantic coast to the Ethiopian highlands (20W-40E, 5N-15N).

© Crown Copyright 2017

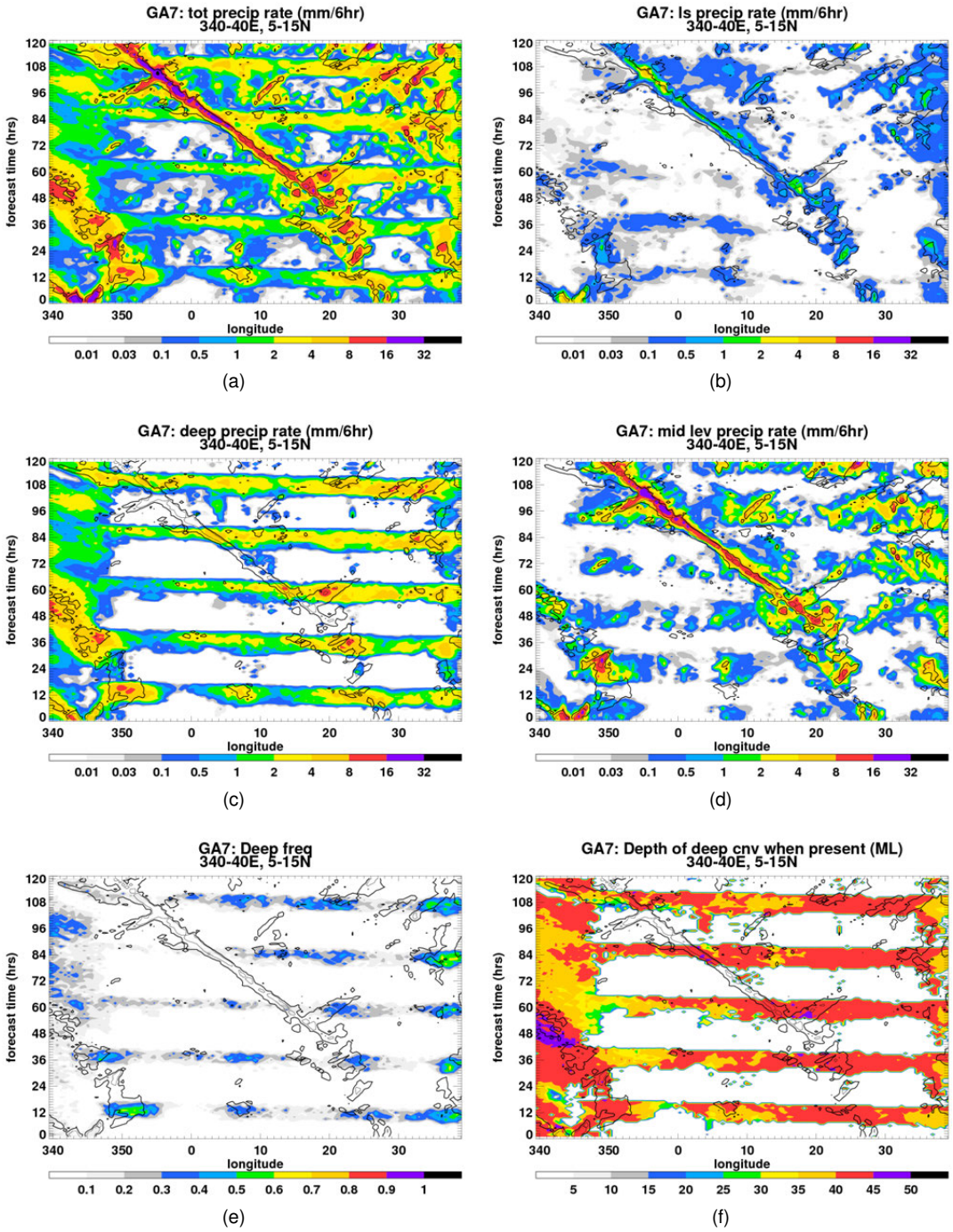

Figure 23: Hovmoller of (a) total precipitation, (b) large-scale precipitation, (c) deep convective precipitation, (d) mid-level convective precipitation, (e) frequency of deep convection and (f) depth of deep convection when present for GA7 N320 case study showing east-west section of Africa from the Atlantic coast to the Ethiopian highlands (20W-40E, 5N-15N). The heavy and light solid black lines show the $0.02\,\mathrm{ms}^{-1}$ and $0.05\,\mathrm{ms}^{-1}$ contour of the $700\,\mathrm{hPa}$ vertical wind from the model and are used to highlight the dynamically active areas.

© Crown Copyright 2017

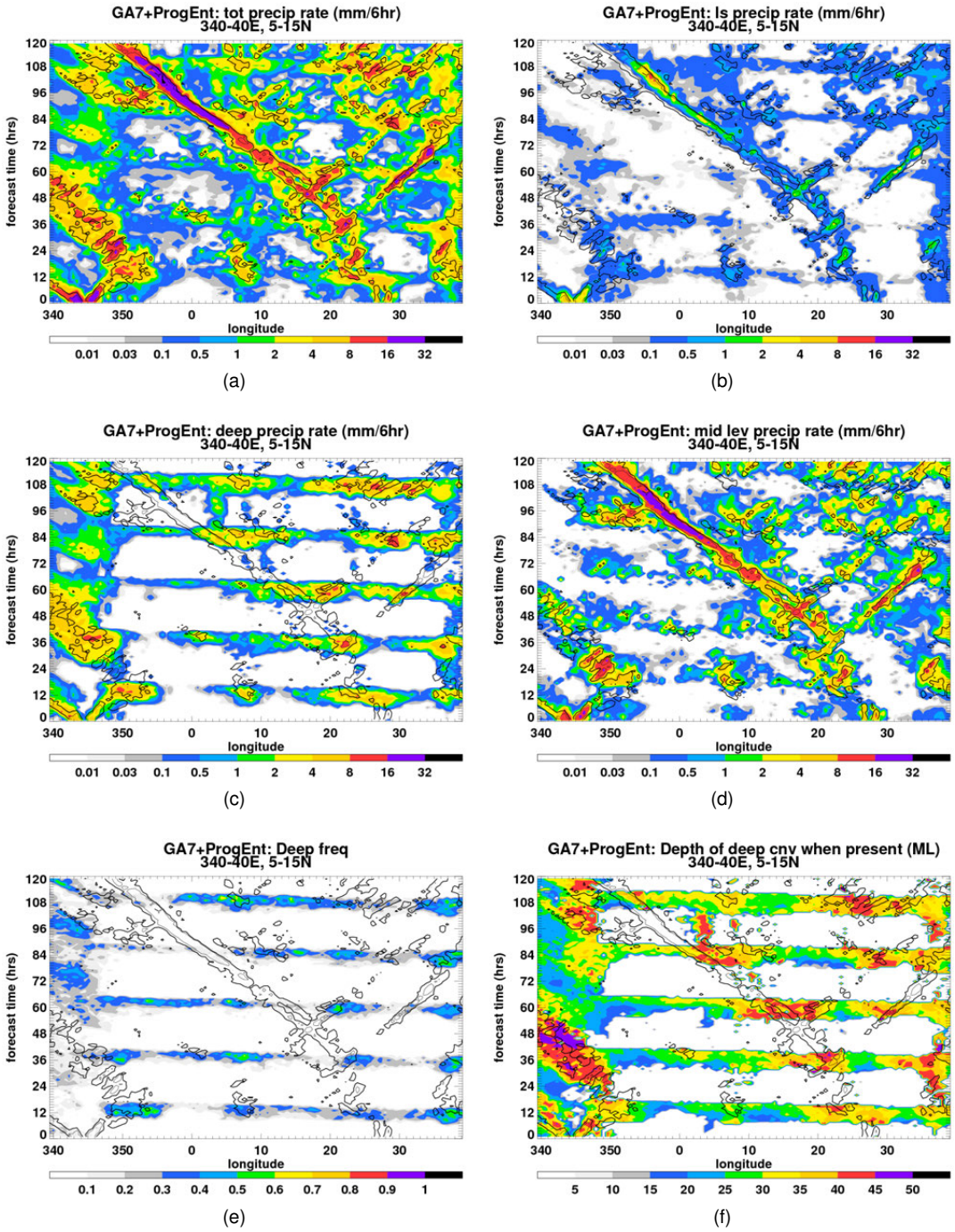

Figure 24: As Figure 23 but for ProgEnt.

© Crown Copyright 2017

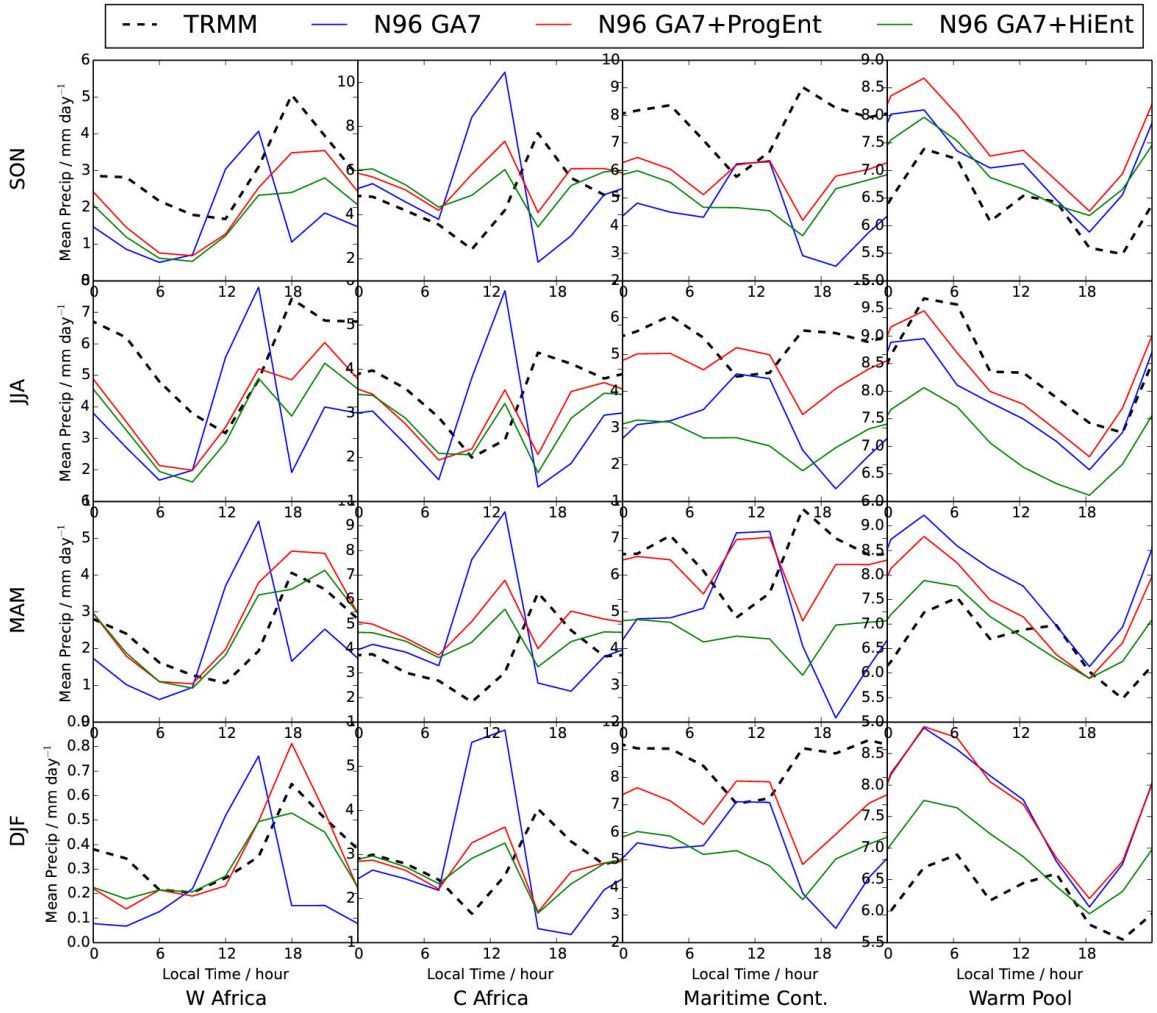

Figure 25: Seasonal mean diurnal cycle of total precipitation for SON (top row), JJA (second row), MAM (third row) and DJF (bottom row) for West Africa, (first column), Central Africa, (second column), the Maritime Continent (third column) and West Pacific warm pool (fourth column). The total precipitation from TRMM (dashed black), GA7 (blue), ProgEnt (red) and HiEnt (green) are shown.

© Crown Copyright 2017

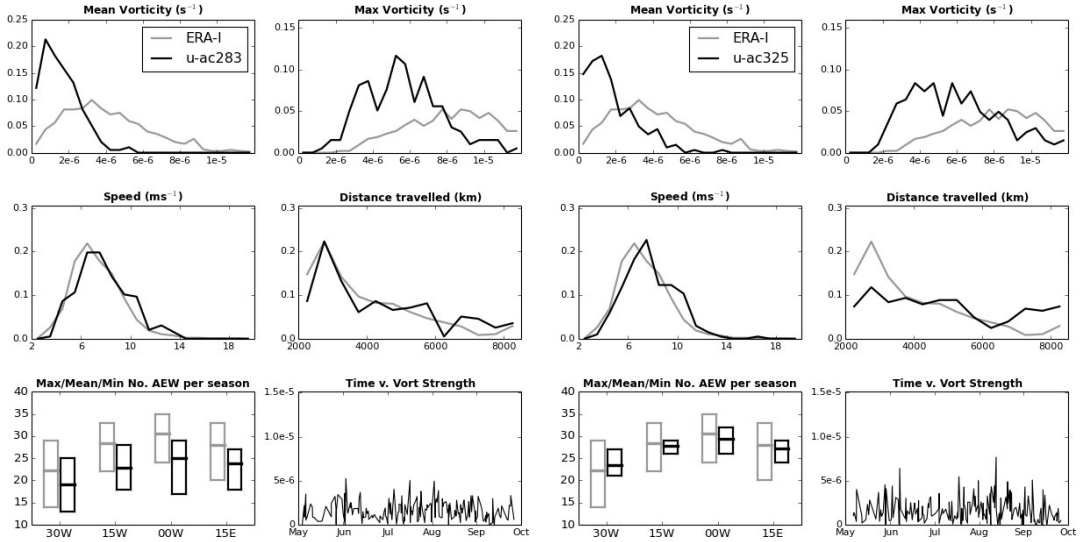

Figure 26: Summary of African easterly wave statistics showing as labelled the histograms of the mean and maximum curvature vorticity at 700hPa, speed, distance travelled, number per season and a sample timeseries of curvature vorticity for (a) GA7 (black) and (b) ProgEnt (black), and for both (a) and (b) ERAI (grey).

© Crown Copyright 2017

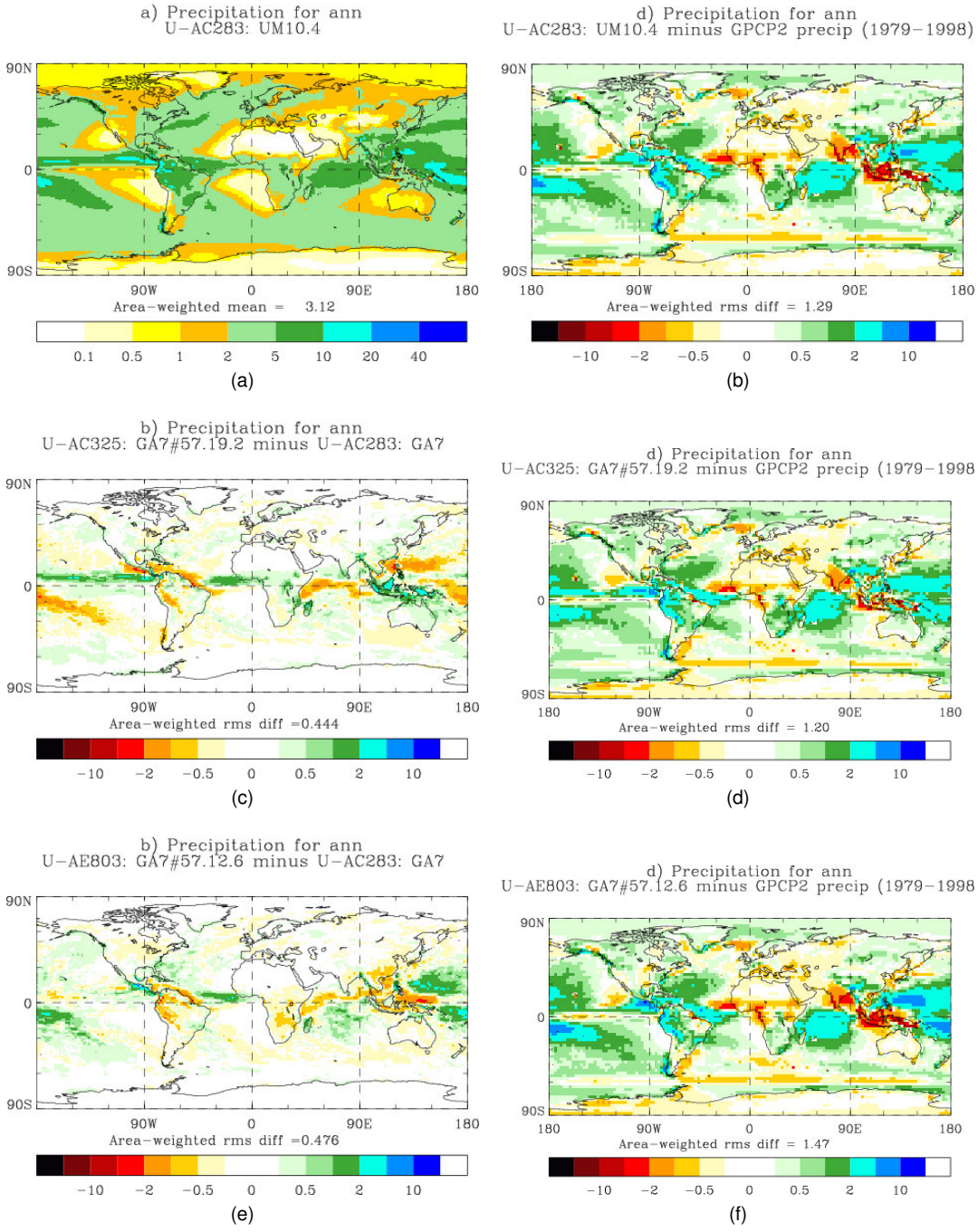

Figure 27: Annual mean precipitation in the 20 yr N96 simulations: (a) GA7, (b) GA7-GPCP, (c) ProgEnt-GA7, (d) ProgEnt-GPCP, (e) HiEnt-GA7 and (f) HiEnt-GPCP.

© Crown Copyright 2017

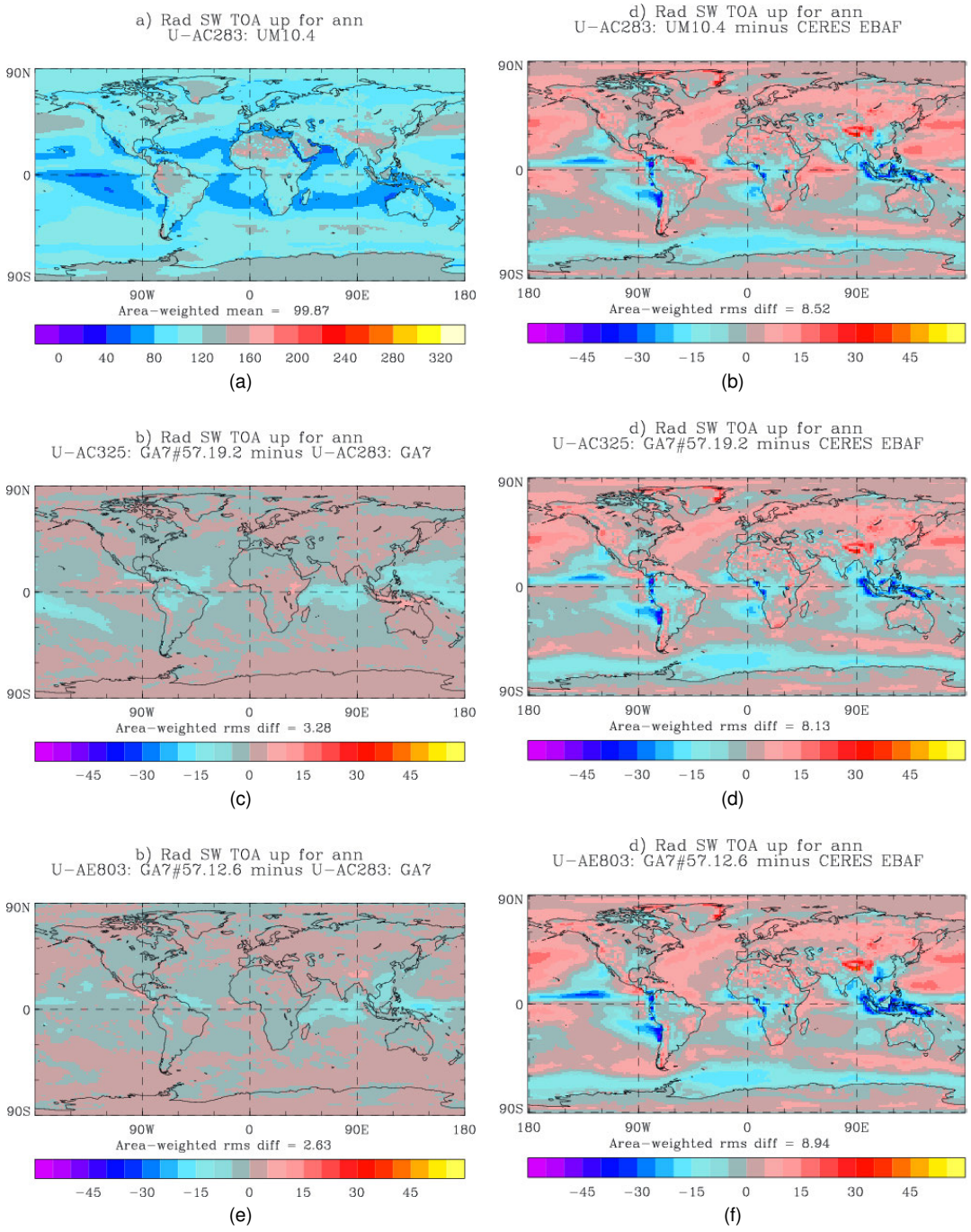

Figure 28: Annual mean outgoing SW in the 20 yr N96 simulations: (a) GA7, (b) GA7-EBAF, (c) ProgEnt-GA7, (d) ProgEnt-EBAF, (e) HiEnt-GA7 and (f) HiEnt-EBAF.

© Crown Copyright 2017

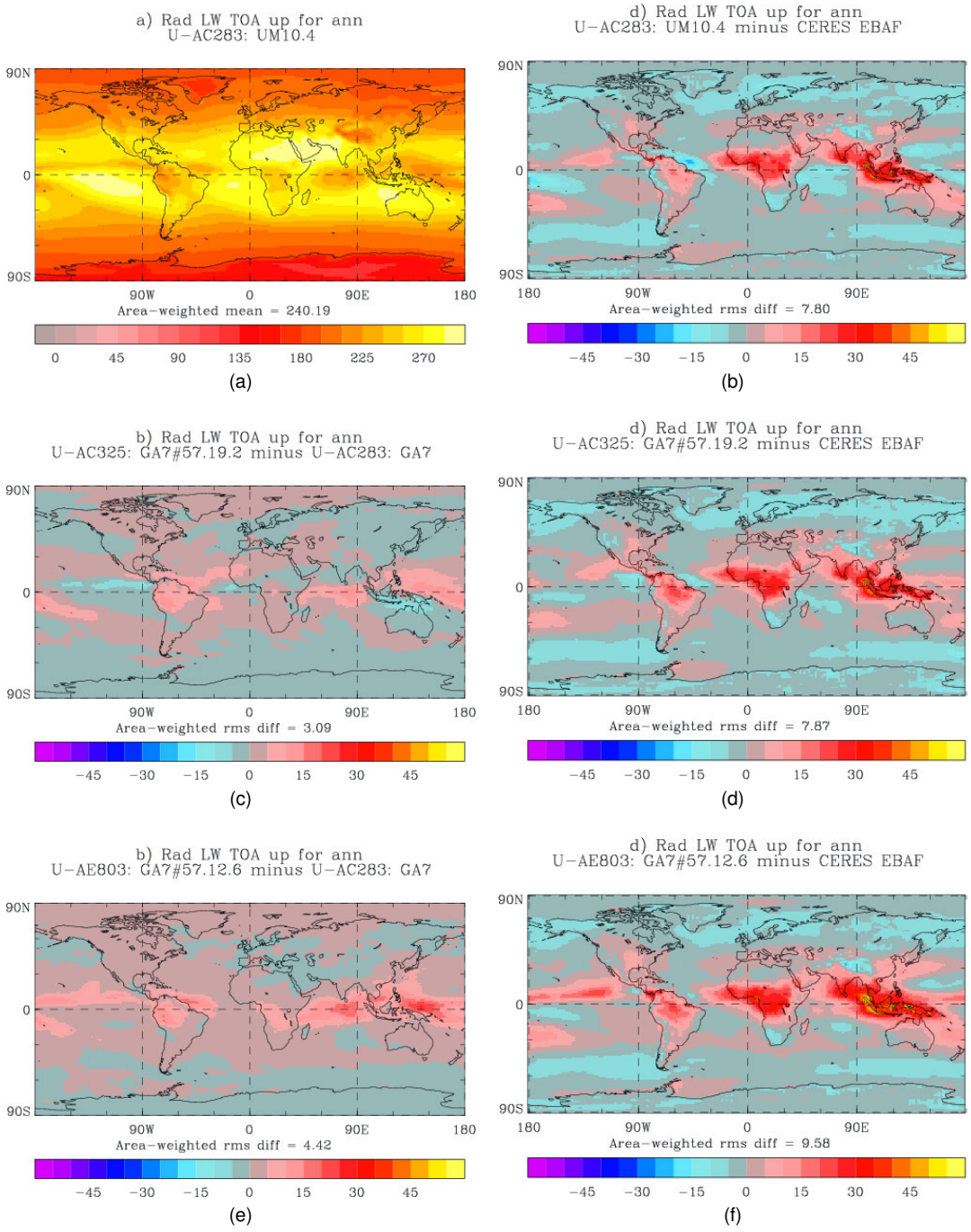

Figure 29: Annual mean OLR in the 20 yr N96 simulations: (a) GA7, (b) GA7-EBAF, (c) ProgEnt-GA7, (d) ProgEnt-EBAF, (e) HiEnt-GA7 and (f) HiEnt-EBAF.

© Crown Copyright 2017

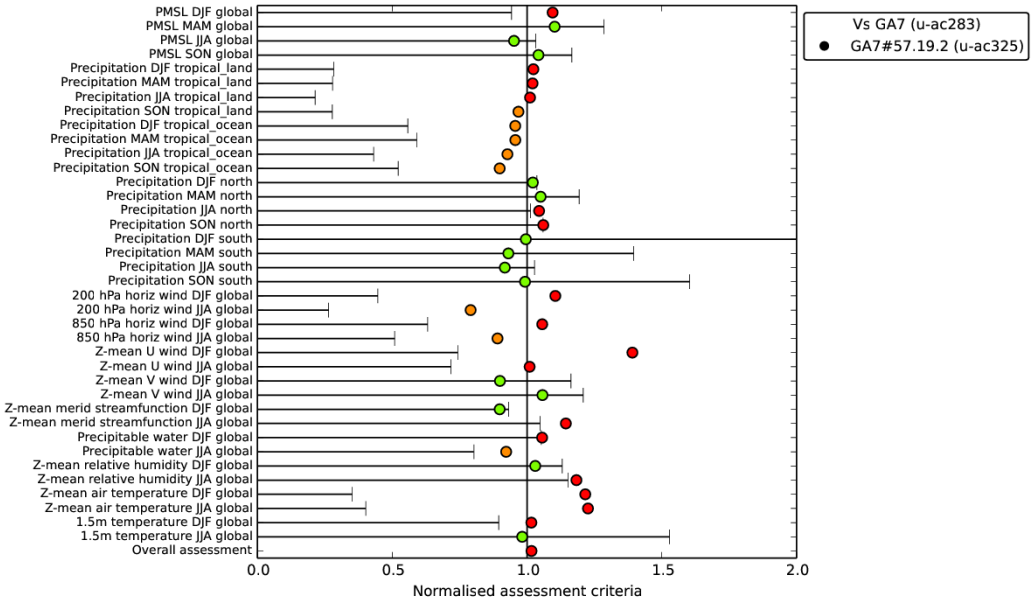

(a)

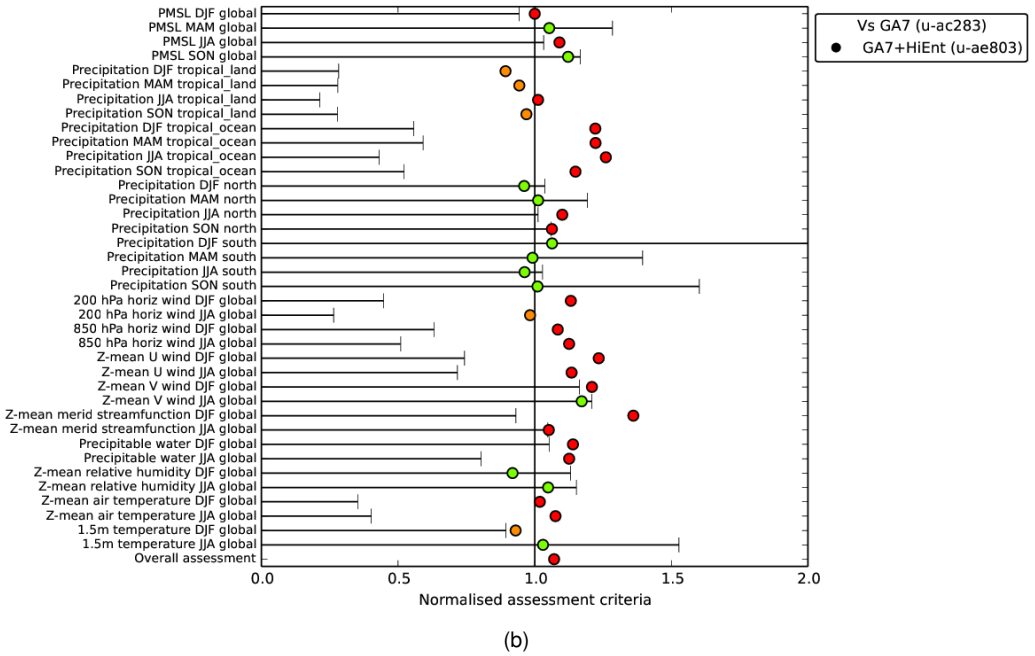

(b)

Figure 30: Global troposphere metrics plot for (a) ProgEnt and (b) HiEnt, both relative to GA7. The metrics are normalised such that those of the GA7 control are equal to 1.0. The error bars indicate the uncertainty in the observations. For each metric, a smaller value implies better agreement with the observed climate.

© Crown Copyright 2017

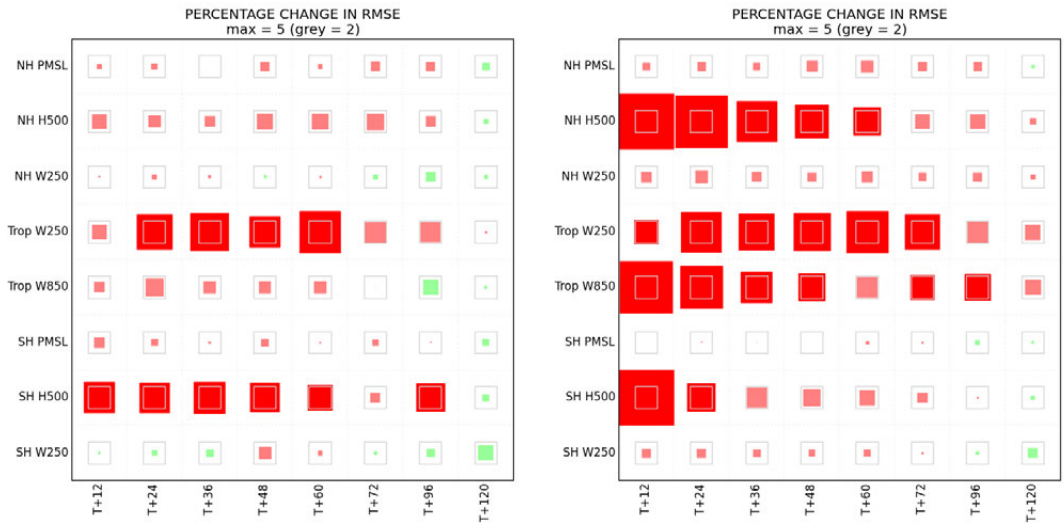

(a) (b)

Figure 31: Global index impact for ProgEnt relative to GA7 with respect to (a) observation and (b) analyses. The size of the squares is proportional to the percentage change in the RMSE and the colour indicates whether RMSE has increased (red) or decreased (green).

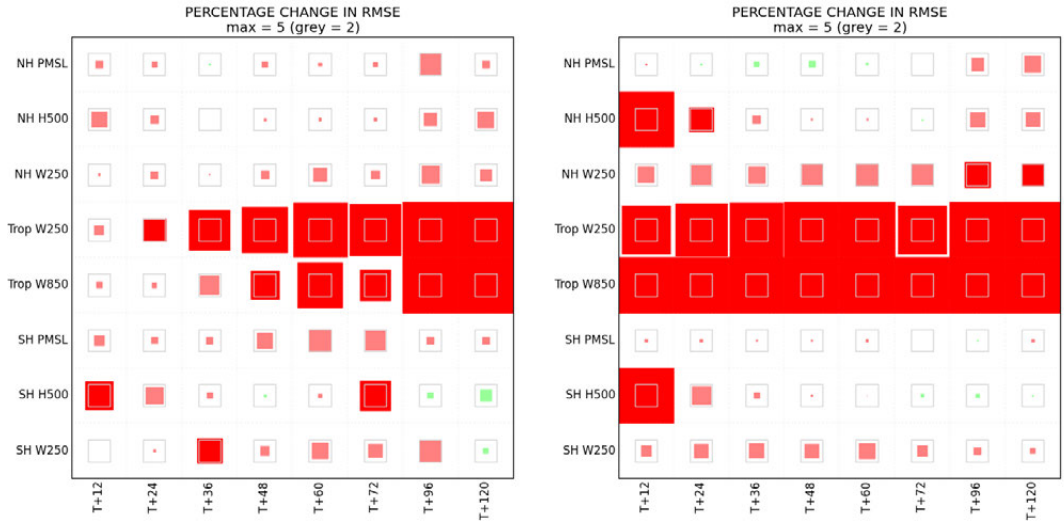

(a) (b)

Figure 32: As figure 31 but for HiEnt

© Crown Copyright 2017

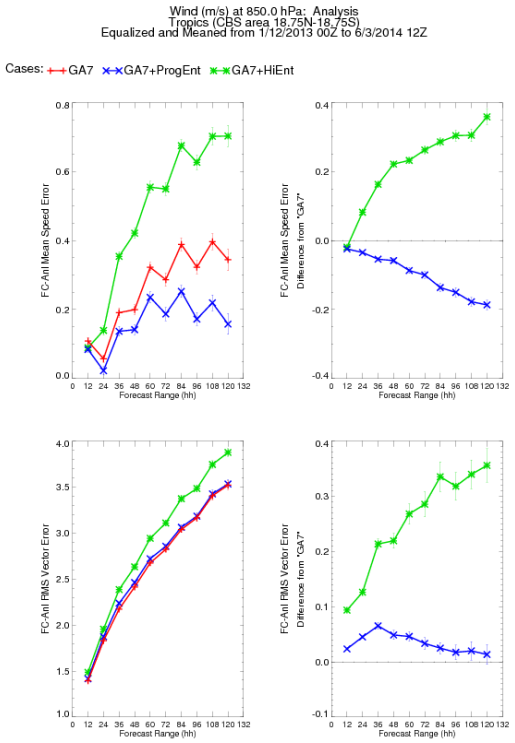

Figure 33: Case study verification of tropical 850 hPa winds from GA7 (red), ProgEnt (blue) and HiEnt (green) relative to analyses. Mean wind speed bias (top left); mean wind speed difference relative to GA7 (top right); root mean square error (bottom left); and difference in rmse relative to GA7 (bottom right).

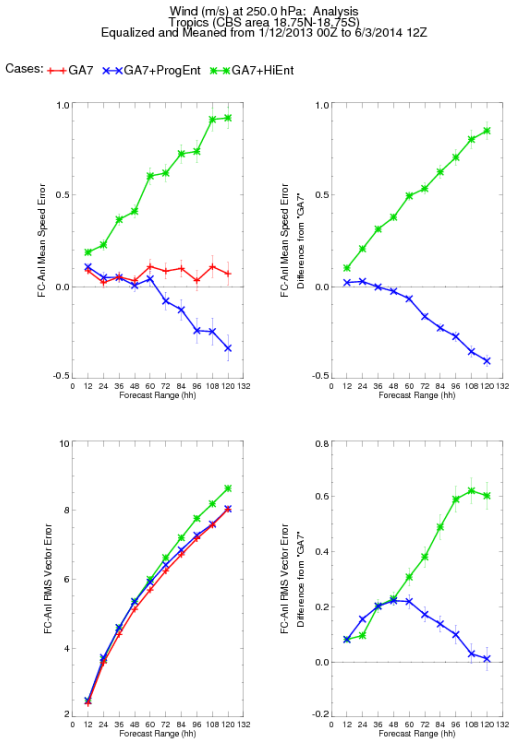

Figure 34: As figure 33 but for tropical 250 hPa winds.

© Crown Copyright 2017

Met Office
FitzRoy Road, Exeter
Devon, EX1 3PB
UK

Tel: 0370 900 0100
Fax: 0370 900 5050
enquiries@metoffice.gov.uk
www.metoffice.gov.uk

Produced with the Met Office LaTeX template v2.0.0